Proposal for the numerical solution of planar QCD

J. Kiskis
Department of Physics, University of California, Davis, California 95616

R. Narayanan
American Physical Society, One Research Road, Ridge, New York 11961

H. Neuberger*
Department of Physics, Technion–Israel Institute of Technology, Haifa 32000, Israel,
School of Physics and Astronomy, The Raymond and Beverly Sackler Faculty of Exact Sciences, Tel Aviv University, 69978 Tel Aviv, Israel,
and Laboratoire de Physique Théorique de l'Ecole Normale Supérieure, 24 rue Lhomond, 75231 Paris Cedex, France
(Received 10 March 2002; published 19 July 2002)

Using quenched reduction, we propose a method for the numerical calculation of meson correlation functions in the planar limit of QCD. General features of the approach are outlined, and an example is given in the context of two-dimensional QCD.

DOI: 10.1103/PhysRevD.66.025019 PACS number(s): 11.15.Ha, 11.15.Pg

I. INTRODUCTION

The phenomenological appeal of planar QCD is well known [1]. It is believed that a limit in which the number of colors N_c goes to infinity while the coupling goes to zero with fixed g^2N_c produces the simpler planar theory while still preserving essential perturbative and nonperturbative features of the physical $N_c=3$ case [2,3]. However, an analytical description of the planar limit has remained elusive. This has left lattice gauge theory as the prevailing approach for the conceptual and quantitative analysis of strong coupling in QCD.

Recent numerical investigations with increasing N_c [4,5] indicate that some $N_c=3$ physical quantities are not far from their $N_c=\infty$ limits. This suggests that numerical results from planar QCD might have phenomenological value. However, in numerical lattice calculations, it is easier to deal with the $N_c=3$ case than to approach the planar limit by simply increasing N_c. An approach that arrives at the simpler planar theory more directly is indicated. The Eguchi-Kawai [6] reduction offers such a shortcut. It has the potential to require much less computation because the planar limit of some observables is obtained from a matrix model with only the $d\times N_c^2$ degrees of freedom of d unitary matrices. Since the dimension d enters linearly rather than exponentially, it seems that four dimensions has only twice the computational cost of two dimensions.

Using the Eguchi-Kawai reduction to approach the planar limit of QCD by first going to infinite N_c and then to zero lattice spacing might be beneficial because the two limits may not commute [7,8]. Also the commutativity of the infinite volume and infinite N_c limits might be questioned because gauge theories are massless, and the construction of [9] does not apply. We begin with the assumption that meson-meson correlation functions at non-zero momenta are "infrared safe." If our calculations in two dimensions are finite and agree with analytical results, then we can be confident about calculations in four dimensions, where infrared problems are less serious.

In the Eguchi-Kawai model the entire d-dimensional lattice is reduced to a point. Nevertheless the matrix model incorporates the lattice structure. This is best understood in momentum space [10], where the d sets of eigenvalues of the link matrices populate the momentum d-torus. To ensure that the torus is indeed covered, one needs to alter the Eguchi-Kawai proposal. The first suggestion for how to achieve this was to freeze the eigenvalue variables and remove them from the integration over gauge fields. The fluctuations of the remaining gauge degrees of freedom are not allowed to back react on the eigenvalue distribution. The expectation value of gauge invariant observables is subsequently averaged over different sets of angles. This produced the quenched Eguchi-Kawai model [10]. Related work on quenched reduced models appeared in [11–13]. A more elegant method, which involves a change in the action by a "twist" [14], was subsequently discovered. This clever approach has also led to the discovery of non-commutative gauge field theories [15] starting from the lattice.

Nevertheless our proposal is in the quenched version [10] because the introduction of fermions in the twisted case is somewhat restricted. The addition of fermions to reduced models was first carried out in a continuum version in [11]. A somewhat similar procedure on the lattice was introduced in [16,17]. In the latter version, the number of flavors N_f was a free parameter and could be taken to infinity. This produces a reduced model leading to the Veneziano limit [18] rather than to the 't Hooft limit [1]. Following up on the idea of [16], a twisted version of the $N_f=N_c$ case was presented in [19]. Since we want to have a variable number of flavors, we opt for the quenched version. In addition, the quenched version is computationally simpler than the twisted one even for $N_f=N_c$ because the Dirac operator is block-diagonal with N_f

*Permanent address: Rutgers University, Department of Physics and Astronomy, Piscataway, NJ 08855.

 ©2002 The American Physical Society

blocks each of size $N_c \times N_c$. In the twisted case, one has a full $N_c N_f \times N_c N_f$ matrix.

Our proposal specifically targets mesonic observables. To get glueball masses from a reduced model, we would need to keep one direction unreduced as described in [20]. To investigate finite temperature, we would again need a Hamiltonian-like formulation [21]. In addition to the calculation of meson masses, our approach allows for the study of fermion quenching effects (valence approximation effects) and finite fermion number density at zero temperature. Also the pathologies of the valence approximation should disappear in the limit of large N_c with fixed N_f. The fermionic bilinears which define the meson fields are the building blocks of the four Fermi operators crucial to the study of weak decays. We envisage taking the $1/N_c$ approach to nonleptonic weak decays [22] to the lattice where it could be compared to more direct approaches and where some of its phenomenological input could be replaced by numerical data obtained from ''first principles.''

There have been both practical and theoretical developments that motivate a return to numerical work on planar QCD. Theoretical progress has led to the new lattice fermions [23], which might be able to solve some problems encountered about 20 years ago [11]. The problems had to do with the meaning of topological charge density in the reduced model, chiral anomalies, and the θ-parameter dependence of the vacuum action density in the planar limit [24]. Equally important are developments in computer hardware. Since the initial numerical experiments on reduced models for planar QCD, computers have become 10^4 times more powerful for fixed power consumption. We suggest that reduced model simulations are a worthy job for weakly (and cheaply) linked PC clusters. Moreover, at infinite N_c, the Wilson-Dirac operator in the argument of the sign function has no small eigenvalues when the pure gauge action of the reduced model is of the usual single plaquette type, and the rescaled lattice gauge coupling is large enough (but not infinite). This is unlike the situation in ordinary QCD [25]. Thus the numerical implementation of the overlap Dirac operator will be simpler than in ordinary QCD.

In Sec. II we define reduced models starting from ordinary formulations of lattice gauge theories. We show that the topological charge remains a nontrivial object even after reduction and that reduced models have, in some sense, more topological numbers than their unreduced counterparts. We briefly discuss chiral gauge theories. The meson-meson correlators, which are the most practical aspect of our proposal, are also introduced. Section III is focused on the special case of two dimensions in which we test the numerical methods. Although planar two-dimensional QCD (QCD_2) has been solved exactly in the weak coupling phase, additional analytical and numerical work is needed to extract the results that can be compared to Monte Carlo data. Although there is a vast literature on QCD_2, in the interest of clarity, we have included a rather detailed account in the Appendix. In Sec. IV we describe some of our ideas for future developments. We believe that there are many options for future research and that the potential for truly new and interesting results is quite high.

II. GENERAL FRAMEWORK

A. Original lattice model and its topological charge

Before reduction, the lattice systems of interest are defined on a d-dimensional hypercubic lattice with a total V sites on a d-torus of equal sides. Sites are labeled by x and positive directions by $\mu = 1,2,\ldots,d$. There are $SU(N_c)$ gauge fields $U_\mu(x)$ on the links, and fermions interact with this gauge background.

Since we are going to deal later with fermions in the fundamental representation, it is best to introduce the fields now, even though we are first focusing on the pure gauge sector. The fermion field ψ is a vector in $V_s \otimes V_c \otimes V_l$, the tensor product of the spin, color, and lattice vector spaces, respectively. Its components are $\psi^i_\alpha(x)$ with spin index α, color index i and lattice position x. There are several operators acting on fermions: The Euclidean Dirac γ_μ's act only on spinorial indices, $\gamma_\mu : V_s \to V_s$. The directional parallel transporters T_μ act on the site index and the group index ($T_\mu : V_c \otimes V_l \to V_c \otimes V_l$) as follows:

$$T_\mu(\psi)(x) = U_\mu(x)\psi(x+\hat{\mu}). \tag{1}$$

For $U_\mu(x)=1$, the T_μ become commuting shift operators T^0_μ. For $V=L^d$ each T^0_μ is unitary and has eigenvalues $e^{(2\pi l/L)k}$, $k=0,1,2,\ldots,L-1$. Hence for even d, T_μ is not only unitary but also has unit determinant [$\det T^0_\mu = (-1)^{d(L-1)}$].

Gauge transformations are characterized by a collection of $g(x) \in SU(N_c)$ acting on ψ pointwise, and only on the group indices. The action is represented by a unitary operator $G(g): V_c \otimes V_l \to V_c \otimes V_l$ with $[G(g)\psi](x) = g(x)\psi(x)$. The T_μ operators are gauge covariant

$$G(g)T_\mu(U)G^\dagger(g) = T_\mu(U^g) \tag{2}$$

with

$$U^g_\mu(x) = g(x)U_\mu(x)g^\dagger(x+\hat{\mu}). \tag{3}$$

The variables $U_\mu(x)$ are distributed according to a probability density that is invariant under $U \to U^g$ for any g.

For the commutators $[T_\mu, T_\nu]$, we have

$$[T_\mu, T_\nu]^\dagger [T_\mu, T_\nu] = (1-P_{\mu\nu})^\dagger (1-P_{\mu\nu}) = 2 - P_{\mu\nu} - P^\dagger_{\mu\nu} \tag{4}$$

with the unitary $P_{\mu\nu}$ given by

$$P_{\mu\nu} = T^\dagger_\nu T^\dagger_\mu T_\nu T_\mu. \tag{5}$$

The operators $P_{\mu\nu}$ are site diagonal with entries that are the parallel transporters around plaquettes:

$$(P_{\mu\nu}\psi)(x) = U_{\mu\nu}(x)\psi(x), \tag{6}$$

$$U_{\mu\nu}(x) = U^\dagger_\nu(x-\hat{\nu})U^\dagger_\mu(x-\hat{\nu}-\hat{\mu})U_\nu(x-\hat{\nu}-\hat{\mu}) \times U_\mu(x-\hat{\mu}). \tag{7}$$

$U_{\mu\nu}(x)$ is associated with the elementary loop starting at site x, going first in the negative ν direction, then in the negative μ direction, and coming back round the plaquette.

The Wilson pure gauge action is given by

$$S_g=\beta\sum_{\mu>\nu} Tr(P_{\mu\nu}+P_{\mu\nu}^\dagger)$$
$$=\text{const}-\beta\sum_{\mu>\nu} Tr[T_\mu,T_\nu]^\dagger[T_\mu,T_\nu]. \tag{8}$$

In the continuum limit, configurations with all the $U_{\mu\nu}(x)$ close to the unit matrix are preferred.

All our operators are finite dimensional matrices. The norm of A is $\|A\|$ with $\|A\|^2$ the largest eigenvalue of $A^\dagger A$. We have

$$\|[T_\mu,T_\nu]\|=\|1-P_{\mu\nu}\|. \tag{9}$$

The gauge invariant constraint

$$\|[T_\mu,T_\nu]\|\leqslant\epsilon_{\mu\nu} \tag{10}$$

for all $\mu>\nu$ does not change the continuum limit. It is equivalent to

$$\|1-U_{\mu\nu}(x)\|\leqslant\epsilon_{\mu\nu} \tag{11}$$

for every site x. The $\epsilon_{\mu\nu}$ are small fixed nonzero numbers, independent of β and of N_c. The probability distribution of the link variables is e^S with integration ranges restricted by Eq. (10).

The lattice version of the massive continuum Dirac operator $D(m)$: $V_s\otimes V_c\otimes V_l\to V_s\otimes V_c\otimes V_l$ is an element in the algebra generated by T_μ, $T_\mu^\dagger$, γ_μ and thus is gauge covariant. The Wilson-Dirac operator $D_W(m)$ is the sparsest possible analogue of the continuum massive Dirac operator which obeys hypercubic symmetry. Fixing the r parameter to its preferred value $(r=1)$,

$$D_W=m+\sum_\mu (1-X_\mu),\quad X_\mu^\dagger X_\mu=1,$$
$$X_\mu=\frac{1-\gamma_\mu}{2}T_\mu+\frac{1+\gamma_\mu}{2}T_\mu^\dagger. \tag{12}$$

One can then prove a general bound [26]

$$[\lambda_{\min}(D_W^\dagger(m)D_W(m))]^{1/2}\geqslant\left[1-(2+\sqrt{2})\sum_{\mu>\nu}\epsilon_{\mu\nu}\right]^{1/2}-|1+m|. \tag{13}$$

Here $\lambda_{\min}(M)$ is the smallest eigenvalue of the matrix M. This bound has content only for m close to -1:

$$|1+m|\leqslant\left[1-(2+\sqrt{2})\sum_{\mu>\nu}\epsilon_{\mu\nu}\right]^{1/2}. \tag{14}$$

This range is contained in the open interval $-2<m<0$.

For even d, we define the Hermitian operator

$$H_W(m)=\gamma_{d+1}D_W(m)\quad\text{for which } H_W^2(m)=D_W^\dagger(m)D_W(m). \tag{15}$$

It follows from Eqs. (10) and (13) that H_W has no zero eigenvalues so that its sign function $\epsilon\equiv\text{sign}(H_W)$ is well defined [27]. The topological charge of a gauge field configuration is given by

$$Q=\frac{1}{2}\text{Tr}\,\epsilon. \tag{16}$$

The value of Q cannot be changed by a smooth deformation that respects the bounds (10). Close to continuum, Q equals the continuum topological charge [28]. The trace in Eq. (16) includes a sum over lattice sites. Leaving this sum out produces a local functional of the lattice gauge background which is a lattice version of the topological charge density $\text{tr}\,F\tilde{F}(x)$. For a review, see [29].

It is important that the proof [26] of the bound makes no use of the special structure of the matrices T_μ in Eq. (1) except their unitarity. Thus any unitary T_μ with commutators close to zero (10) can be used in Eqs. (12) and (16) to define homotopy classes for the gauge backgrounds. Of course, the ''local'' topological density has no meaning if the T_μ's are that general.

Although we spoke about fermions and used gamma matrices, they were auxiliary concepts. We only dealt with the pure gauge sector. The gamma matrices played a role in defining the topological number, but the latter is just a function of the gauge field background. It will be important in the following discussion that this definition of Q can be non-zero on a finite lattice. One need not to go to an infinite lattice to see non-zero topology.

B. Reduced model and reduced topological charge

The reduced model for lattice gauge fields [6] is defined on a toroidal lattice with a single site. The matrices T_μ become unitary matrices with no restrictions on their structure since they are equal to U_μ [cf. Eq. (1)] on a single site lattice. A connection between models differing only in the number of sites V can be established by taking N_c to infinity with β/N_c fixed. The leading behavior of traces of Wilson loops written in terms of the T_μ is then independent of V. Actually this is only true for β/N_c small enough. It fails for large β/N_c and thus also for the continuum limit [10]. The key to fixing the model is to understand that the V independence is caused by momentum space getting absorbed into the space of eigenvalues of the operators T_μ. Consequently, the quenched reduced lattice model is defined by freezing the eigenvalues of T_μ to a set uniformly distributed over the unit circle for each μ [10],

$$T_\mu = V_\mu D_\mu V_\mu^\dagger, \quad D_\mu = \mathrm{diag}(e^{i\theta_\mu^1}, e^{i\theta_\mu^2}, \ldots, e^{i\theta_\mu^{N_c}}). \tag{17}$$

The angles θ_μ^i are randomly distributed in the interval $[-\pi, \pi]$. The ordering of the angles for each direction μ does not matter since one can go from one ordering to another by appropriately changing the integration variables V_μ. In other words, only the sets of eigenvalues are frozen, not the ordering within each set. The matrices V_μ are unitary and otherwise restricted only by Eq. (10).

The pure gauge action is invariant under $V_\mu \to V_\mu D'_\mu$ where the D'_μ are arbitrary diagonal unitary matrices. Thus the V_μ should be thought of as taking values in the coset space $U(N_c)/(U(1))^{N_c}$. The most important symmetry of the pure gauge action is gauge invariance which now acts by conjugation $T_\mu \to \Omega T_\mu \Omega^\dagger$. One can think of Ω as the replacement for $G(g)$ in Eq. (2). The gauge group is $SU(N_c)/Z(N_c)$.

The absolute minima of the action are given by T_μ's that are simultaneously diagonal. These minima are changed one into another by certain sets of V_μ matrices. In the double line notation [10–13] of planar graphs, the crystal d momentum going through a line is given, component by component, by the difference between the angular phases of the two eigenvalues of T_μ associated with each of the color indices attached to each component of the double line. Different minima give different momenta, and the sum over minima together with the sum over color indices reproduces the ordinary planar lattice Feynman diagrams. As the typical spacing between a θ_μ^i and the closest θ_μ^j is of order $1/N_c$, it follows that the momenta values are in effective correspondence with those in a finite volume of size $V = N_c^d$. On the other hand, focusing on a single minimum might suggest $V = N_c$. In the twisted case, one typically gets $V = N_c^{d/2}$. In numerical simulations, it is important to ensure that all minima are properly sampled.

In the continuum version of the reduced model [11], the basic variables are traceless Hermitian matrices A_μ with restrictions on their eigenvalues. One could try a ''geometric'' definition of topological charge, but it does not work well [11]. The natural expression corresponding to the non-Abelian field strength is $F_{\mu\nu} = [A_\mu, A_\nu]$. So long as the A_μ are finite matrices,

$$\mathrm{Tr}\, F\tilde{F} \propto \epsilon_{\mu\nu\rho\sigma} \mathrm{Tr}\, A_\mu A_\nu A_\rho A_\sigma = 0 \tag{18}$$

because of the cyclicity of the trace and the antisymmetry of the epsilon symbol. To get non-zero topological charge, one needs to work with infinite A_μ matrices, and a numerical approach seems impossible. The topological charge of the lattice reduced model is defined by Eq. (16) using unitary T_μ's that are restricted only by Eq. (10). As already mentioned, the definition of topological charge and the restriction on the commutators (10) work exactly the same way as before.

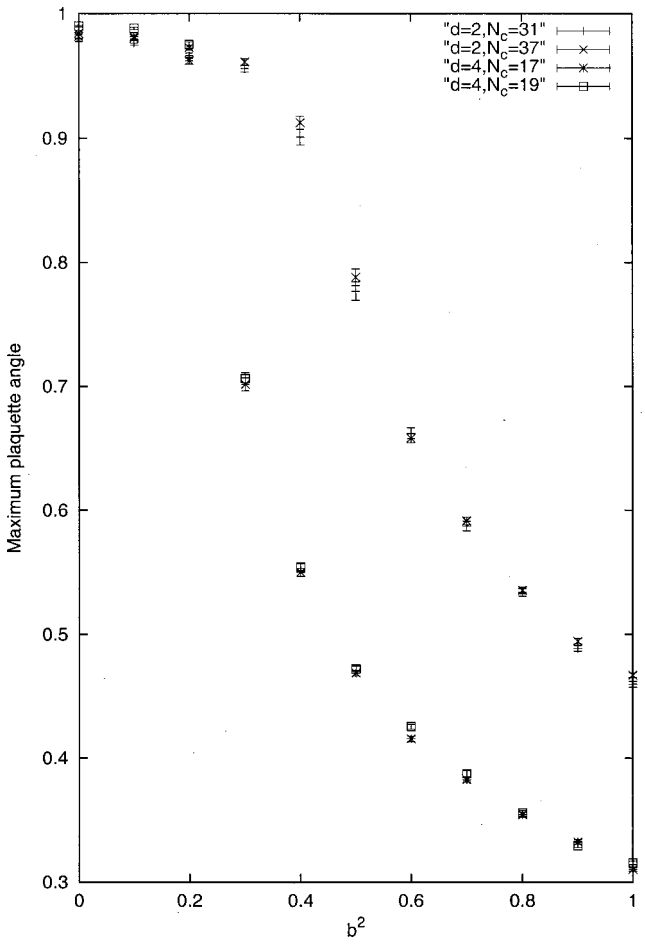

FIG. 1. Plot of the maximum plaquette angle in units of π as a function of $b^2 = \beta/N_c$. The data are at $N_c = 31$ and $N_c = 37$ for the two-dimensional model and are at $N_c = 17$ and $N_c = 19$ for the four-dimensional model.

This extra constraint (10) on the commutators of T_μ is not necessary at infinite N_c. For $d = 2$, when we get close enough to the continuum limit and the lattice gauge coupling $b^2 = \beta/N_c$ is large enough, we are far below the Gross-Witten phase transition [30], and the plaquette eigenvalue distribution is contained in a small neighborhood of unity. This is evident in Fig. 1 where we have plotted the expectation value of the maximum angle of the untraced plaquette in units of π for two different values of N_c in the quenched model. This is also true in four dimensions where again there is a phase transition as seen in the Fig. 1. A similar result was also found in the four-dimensional twisted Eguchi-Kawai model [31]. The numerical evidence strongly indicates that the extra condition restricting the matrices is satisfied as long as we are close enough to continuum even if we use only the simplest single plaquette Wilson action.

A complete study of topological charge is beyond the scope of this paper and our discussion will be brief. Consider a two-dimensional gauge field background in which the T_μ's represent a $U(1)$ background that is a $U(1)$ instanton on a two-dimensional torus. The T_μ have the structure of a ''shift'' and a ''clock'' matrix [32]:

$$T_1 \equiv X = \begin{pmatrix} 0 & 1 & 0 & \dots & 0 \\ 0 & 0 & 1 & \dots & 0 \\ \dots & \dots & \dots & \dots & \dots \\ 0 & 0 & \dots & 0 & 1 \\ 1 & 0 & \dots & 0 & 0 \end{pmatrix} \quad (19)$$

$$T_2 \equiv Y = \begin{pmatrix} 1 & 0 & 0 & \dots & 0 \\ 0 & \zeta & 0 & \dots & 0 \\ 0 & 0 & \zeta^2 & \dots & 0 \\ \dots & \dots & \dots & \dots & \dots \\ 0 & 0 & \dots & 0 & \zeta^{N-1} \end{pmatrix}. \quad (20)$$

Here $\zeta = e^{2\pi i/N_c}$, and we take $N = N_c$. This Abelian background on a lattice of area N_c can be viewed as a non-Abelian $SU(N_c)$ background in the reduced model. As far as the spectra of the various lattice Dirac operators go, how we look at the background is irrelevant. Hence, the reduced model has $Q=1$ for this configuration. Moreover, calculating the gauge field action, we easily can check that it stays finite in the 't Hooft large N_c limit. Similarly, one can easily check that Eq. (10) is satisfied for N_c beyond some finite value.

One expects no topological effects in two-dimensional planar QCD. This is not in contradiction with our observation because the continuum limit is obtained when the fixed parameter of the 't Hooft limit β/N_c is taken to infinity, and these backgrounds do not contribute. We learn that lattice reduction may perform a ''miracle'' in the sense that one may find topological effects that were not present in the original continuum model. Whether or not these effects are relevant in the continuum limit is a dynamical question.

What happens in four dimensions? We have seen that what looks like an Abelian background before reduction can appear as a non-Abelian background in the reduced model. (Actually, the results of [33] say that for any finite $N_c \geqslant 3$ on a continuous torus, any allowed value of Q can be attained by an Abelian background. We are not making use of that result here.) In four dimensions, one can obtain a configuration that is nontrivial topologically, for example, by choosing an Abelian instanton in the 1-2 plane and another Abelian instanton in the 3-4 plane. These instantons would lead to shift-clock pairs as above. We could take $N_c = N^2$ and write the T_μ's as direct products of $N \times N$ matrices: $T_1 = X \otimes 1$, $T_2 = Y \otimes 1$, $T_3 = 1 \otimes X$ and $T_4 = 1 \otimes Y$. All these matrices are in $SU(N^2)$. The topological charge of this background is $Q=1$. The spectra of the T_μ's are highly degenerate in this example. To produce truly acceptable configurations in a quenched reduced model, we would need to find deformations of these matrices that lift the degeneracy while preserving $Q=1$.

The action of this configuration diverges linearly with N_c, just like the action of a continuum instanton. But we see that there are configurations with non-zero Q, and the question of their survival at infinite N_c is similar to the familiar question in the continuum [34]. This indicates that in four dimensions, the reduced lattice model could provide a framework in which one can at least pose questions about topology at infinite N_c. This is interesting because the results of Teper [4] support a finite nonvanishing limit to the topological susceptibility in the lattice planar limit. We do not know if there are configurations that produce $Q=1$ and have an action that stays finite as N_c goes to infinity.

We now make an observation that might be of relevance to the issue of θ dependence in the planar limit. The set of backgrounds satisfying Eq. (10) falls apart into non-empty disconnected components beyond what is needed for distinct topology. Even at fixed Q there are several components. These different components make separate contributions to the partition function, and these contributions are not obviously suppressed at infinite N_c. It could be that the particular connected component that dominates at infinite N_c depends discontinuously on parameters, and therefore the action density need no longer be differentiable with respect to its parameters. In particular, this could induce a nonanalyticity in θ/N_c, and this might be a way of reconciling the naive scaling for the action density $[\sim N_c^2 f(\theta/N_c)]$ with 2π periodicity in θ [24].

To see that the set of gauge fields one integrates over splits into disconnected components, consider again the above two-dimensional example. Complete the pair $T_{1,2}$ by a T_3 and a T_4 of a perturbative nature so that $Q=0$. The shift-clock pair cannot be deformed smoothly to unity while obeying the constraint on the commutator because the shift-clock pair could be used to construct a two-dimensional lattice Dirac operator which would have a two dimensional topological charge of unity. Thus, this set of four T_μ's has $Q=0$ but is homotopically inequivalent to a set where all four T_μ's are perturbative and consequently also has $Q=0$. In spite of the fact that we are considering only $SU(N_c)$ and not $U(N_c)$, the two-dimensional Chern numbers associated with the different two-dimensional tori included in the four-dimensional torus manage to survive in the reduced model.

Let us briefly mention anomalies associated with chiral fermions. The free energy of the reduced model with fermions included is supposed to reproduce the free energy of the original model at leading order N_c^2 and subleading order N_c. Hence, anomalies should spoil the gauge invariance of the reduced model too. In the overlap formalism, there are simple lattice Abelian gauge backgrounds [35] in which one can prove that gauge invariance cannot be preserved if there are anomalies in the continuum. Moreover, this happens already on finite lattices. These backgrounds can be ''borrowed'' to produce non-Abelian backgrounds in the reduced model with a similar effect. The overlap line bundle is twisted over the torus defined by variables $|p_{1,2}| \leqslant \pi$ that enter through the family of gauge backgrounds described by $T_1 = e^{ip_1} \otimes Y$, $T_2 = e^{ip_2} \otimes Y$, $T_3 = X \otimes 1$, $T_4 = Y \otimes 1$ and, as in the case of the ''instanton,'' $N_c = N^2$. Again, we see the potential to move beyond the obstacles identified in [11], but there is a degeneracy of eigenvalues we need to eliminate.

C. Fermions

In the original unreduced lattice model, massless fermions are incorporated through the massless overlap Dirac operator [27]

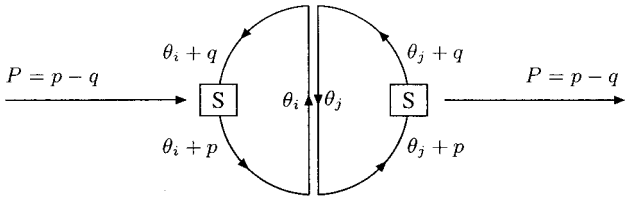

FIG. 2. A planar diagram representing the one gluon exchange contribution to the scalar-scalar correlation at momentum P.

$$D_o = \frac{1}{2}(1 + \gamma_{d+1}\epsilon) \tag{21}$$

with $\epsilon = \mathrm{sign}(H_W)$. The operator D_o has an implicit dependence on the fermion parallel transporter.

The reduced version of D_o is obtained by replacing the original transporter with the reduced fermion parallel transporter. For fermion momenta $-\pi < p_\mu \leqslant \pi$ and T_μ given in Eq. (17), the reduced transporter is $e^{ip_\mu}T_\mu$. With that replacement, D_o becomes the reduced massless overlap Dirac operator. It depends on the fermion momentum. The external line propagator [36] is

$$g(p) = \frac{1}{2m}[D_o^{-1} - 1]. \tag{22}$$

Consider the connected correlation function of the fermion bilinear $(1/\sqrt{N_c}), \overline{\psi}(x)\psi(x)$. In momentum space it is given by

$$G(P) = -\frac{1}{N_c}\langle[\langle \mathrm{Tr}\, g(p)g(q)\rangle_{\text{gauge average}}]\rangle_{\text{angle average}} \tag{23}$$

with $P = p - q$. Similar expressions can be derived for the correlation functions of other bilinears.

The way reduction works is best understood by looking at an example. Figure 2 is a diagram showing the various momenta in the one gluon exchange contribution to a scalar-scalar correlator. All crystal momenta come from the diagonal entries of the fermion transporter and flow in the directions indicated by the arrows. The θ momenta are associated with color and the p,q momenta with flavor. Single lines are fermions, and the double line is the exchanged gluon. The gluon carries momentum $\theta_i - \theta_j$. With the quenched θ_i randomly distributed on the momenta tori, the summation over the color indices i and j induces the needed integrations over momenta.

Note that we compute the meson correlators directly in momentum space. This is an important new feature with several potential applications.

When the quarks are massive, the propagator $g(p)$ is [37]

$$g(p) = \frac{1}{2m}\,\frac{1 - \gamma_{d+1}\epsilon}{(1+\mu) + (1-\mu)\gamma_{d+1}\epsilon}. \tag{24}$$

The parameter μ fixes the bare lattice quark mass via $m_q = 2m\mu$.

The transporter $e^{ip_\mu}T_\mu$ introduces a phase into the reduced fermion operator. This suggests that there are several options for defining Q, something we glossed over in Sec. II B. It is a bit strange that one seems to be able to define a topological charge that depends on the momentum carried by the fermions. Probably, for configurations typical to the continuum limit, Q ends up not depending on p. This is indeed the case for examples in Sec. II B as long as N is large enough and the momenta are not too large.

It is quite easy to add N_f flavors of fermions and then go to the topological limit $N_f, N_c \to \infty$ with N_f/N_c kept fixed. In this limit the fermionic determinant needs to be included in the gauge field integration. Similarly, one can also introduce fermions in representations other the fundamentals. Chiral gauge theories will have anomalies because, as mentioned before, the backgrounds that produce them have a reduced model representative [35].

III. TWO-DIMENSIONAL PLANAR QCD

As an exercise, we will calculate the scalar-scalar

$$\langle \overline{\psi}(x)\chi(x)\overline{\chi}(0)\psi(0)\rangle \tag{25}$$

and the pseudoscalar-pseudoscalar

$$\langle \overline{\psi}(x)\gamma_3\chi(x)\overline{\chi}(x)\gamma_3\psi(0)\rangle \tag{26}$$

correlation functions in momentum space in the planar limit of two-dimensional QCD. (We use two different fields, ψ and χ, to eliminate the disconnected piece.) These correlation functions are known exactly and are completely determined by their Feynman diagrams. Nevertheless, they are quite nontrivial. While they can be expressed as an infinite sum over stable mesons with mass squares that are evenly spaced asymptotically, they also have free field behavior at large momenta. Thus, we have the cohabitation of asymptotic freedom and total confinement that is also present in four-dimensional planar QCD. Moreover, with an appropriate choice of limits, chiral symmetry is broken, and there a Goldstone boson. If the potential infrared problems turn out to be tractable in two dimensions, we can be confident that there will not be any difficulties in four dimensions where infrared issues are less serious.

In two-dimensional QCD, spontaneous chiral symmetry breaking only occurs if one takes the limit $m_q \to 0$ after the planar limit $N_c \to \infty$ at fixed β/N_c. In the reduced model for any finite N_c, we have exact chiral symmetry at $m_q = 0$, and we can investigate the planar limit of the massless reduced model. The continuum limit is taken last. With m_q set to zero before the large N_c limit, we will not see direct signals of spontaneous symmetry breaking. The simplest assumption is that chirally invariant quantities will be well described by 't Hooft's solution, but chirally noninvariant observables will not be. Thus the invariant combination to compare to the 't Hooft solution is

$$\langle \overline{\psi}(x)\chi(x)\overline{\chi}(0)\psi(0)\rangle - \langle \overline{\psi}(x)\gamma_3\chi(x)\overline{\chi}(0)\gamma_3\psi(0)\rangle. \tag{27}$$

For massive quarks, the situation is less subtle, and one can consider the correlators separately. The planar limit of the reduced model is supposed to produce a UV regulated approximation to the 't Hooft solution. It is interesting to see in detail how this works. On the one hand, the very high mass mesons are meaningless entities at finite ultraviolet cutoff, while on the other hand, they are responsible for the free field short distance behavior.

It is believed that ordinary, massive two-dimensional QCD has two phases [38]: a weak coupling one in which the gauge coupling divided by the quark mass is small and a strong coupling one in which this ratio is large. In the strong coupling phase, there are light baryonic states, but there is no pion whose mass vanishes as $\sqrt{m_q}$ in the chiral limit, and it is not clear how the large N_c limit should be defined. 't Hooft's planar solution is in the weak coupling phase and does have a pion mass that vanishes as $\sqrt{m_q}$. It is interesting that the numerical results obtained in [5] seem to correspond to the strong coupling phase and, nevertheless, also seem to admit a large N_c limit with the 't Hooft scaling of the gauge coupling. Thus it could be that in two-dimensional QCD there exists a strong coupling planar phase that is defined through the lattice and which differs from the 't Hooft's solution.

We will work in the weak coupling phase where 't Hooft's solution should be valid. If there are indeed two planar phases, convergence to the planar continuum limit of the weak coupling phase might be slower than anticipated.

A. Pure gauge

We can go to a ''unitary gauge'' in which T_2 is fixed to the clock matrix Y, with $N=N_c$. Denoting T_1 by U the partition function is

$$Z=\int_{U=WYW^\dagger,\quad W\in U(N)} dW e^S,$$
$$S=4\beta\sum_{ij}\ |U_{ij}|^2\sin^2\frac{\pi(i-j)}{N_c}. \tag{28}$$

Terms with $i=j$ do not contribute to S. All absolute minima of S are at $U^\sigma_{ij}=\delta_{ij}e^{2\imath\pi\sigma_i/N_c}$. Here σ is a permutation of $0,1,2,\ldots,N_c-1$. There are no other minima.

For very large β/N_c, the relative weights of distinct minima are given by the ratios of determinants of small fluctuations around the configurations. We parametrize the fluctuating degrees of freedom by the off-diagonal entries of a Hermitian matrix H which generates a conjugation around a diagonal saddle:

$$\delta U_{ij}=i[U^\sigma,H]_{ij}=iH_{ij}[e^{2\imath\pi\sigma_j/N_c}-e^{2\imath\pi\sigma_i/N_c}]. \tag{29}$$

The diagonal terms of U do not contribute, and the second order action is

$$\delta^2 S=16\beta\sum_{ij}\ |H_{ij}|^2\sin^2\frac{\pi(\sigma_i-\sigma_j)}{N_c}\sin^2\frac{\pi(i-j)}{N_c}. \tag{30}$$

Since

$$\prod_{i\neq j}\left|\sin\frac{\pi(\sigma_i-\sigma_j)}{N_c}\right|=\prod_{i\neq j}\left|\sin\frac{\pi(i-j)}{N_c}\right| \tag{31}$$

for any permutation σ, all minima should be visited with equal frequency for large β/N_c.

One may ask whether the barriers between different minima are high and whether they become infinite in the large N_c limit. The minima can be connected by sequences of transpositions. We do not know whether the barriers are infinite at infinite N_c and whether in two dimensions, where the Feynman diagrams capture all the physics, one can ignore the many minima.

From now on, we will use $b=\sqrt{\beta/N_c}$ as the parameter held fixed as N_c goes to infinity. In the planar limit, one approaches the continuum limit (and hopefully the 't Hooft solution) when $b\to\infty$. Comparing to a continuum definition of the gauge coupling where the partition function is given by

$$\exp\left\{-\frac{1}{4g^2}\sum_{\mu\nu}\ \mathrm{Tr}\,F^2_{\mu\nu}\right\}, \tag{32}$$

we get

$$g^2=\frac{1}{2\beta}=\frac{1}{2N_c b^2}. \tag{33}$$

To get a feeling for the numbers, consider two-dimensional QCD with massless quarks. The lowest scalar meson mass is approximately $0.967/b$. In taking a sequence of increasing β's and N_c's with $b^2=5$, we find that this mass approaches 0.43 in lattice units. With a mass scale this large in lattice units, we can expect good agreement with the continuum theory only for small momenta.

In two dimensions, quenching is not necessary [10,39]. We will use a version of the model where there is no longer a need to perform the average over the angles. In this version the eigenvalues of the T_μ matrices are still frozen to the set consisting of the N_c roots of unity. This adds a new ''translational'' symmetry to the model in which each T_μ is replaced by $z_\mu T_\mu$ with $z_\mu^{N_c}=1$. This transformation preserves the eigenvalue sets. With N_c chosen to be a prime number, the eigenvalues of T_μ^k will span the same roots of unity for any $0\leqslant k\leqslant N_c-1$, and will simulate the situation on a torus of size N_c^2.

Let us summarize the symmetries of the bosonic action:

$$S_g(T_1,T_2)=S_g(z_1T_1,z_2T_2)\quad\text{with } |z_\mu|=1$$
$$S_g(T_1,T_2)=S_g(T_1^\dagger,T_2)=S_g(T_1,T_2^\dagger) \tag{34}$$
$$S_g(T_1,T_2)=S_g(T_2,T_1).$$

These symmetries reflect invariances of the original toroidal lattice theory.

B. Fermions and meson observables

The fermionic momenta p_μ can be chosen from the set $2\pi j/N_c$, $j=0,1,\ldots,N_c-1$ for fermions with periodic boundary conditions and from the set $j=\frac{1}{2},\frac{3}{2},\ldots,N_c-\frac{1}{2}$ for fermions with anti-periodic boundary conditions. Thus, the momenta flowing in the fermion lines are identical in type to those flowing in the gauge boson lines. With these momenta, the planar Feynman diagrams are similar to those of a system on a lattice with N_c^2 sites.

The symmetries of Eq. (34) imply that the meson field propagators (23) obey the following relations:

$$G(P_1,P_2)=G(-P_1,P_2)=G(P_1,-P_2)=G(-P_1,-P_2)$$
$$G(P_2,P_1)=G(P_2,-P_1)=G(-P_2,P_1)=G(-P_2,-P_1). \tag{35}$$

These symmetries will be strictly enforced by explicitly adding the contributions of all gauge field configurations connected by the symmetry transformations of Eq. (34).

G will be denoted by S for the scalar meson propagator and by P in the pseudoscalar case. 't Hooft's solution, together with subsequent work [40], provide explicit formulas for S and P in momentum space. Since they are composite, there are ultraviolet divergences, and the unrenormalized formulas are divergent. Since their source is in free field theory, these divergences can be regulated in many ways. We define the renormalized meson correlators S_R and P_R by subtracting at zero momentum for massive quarks and at an arbitrary momentum point for massless quarks.

The continuum results we strive to reproduce using our reduced model are expressed in terms of the eigenvalues and eigenfunctions of 't Hooft's Hamiltonian H. It acts on square integrable functions defined on the interval $[0,1]$. The boundary conditions are Dirichlet for massive quarks and von Neumann for massless quarks. For massive quarks, H is positive definite. For massless quarks, it has one eigenstate with zero eigenvalue, and all other eigenvalues are strictly positive. There are no degeneracies, and the eigenvalues of H provide the masses squared of the meson bound states. In the following discussion, all dimensionful quantities are converted to their dimensionless counterparts using the scale

$$e^2 \equiv \frac{g^2 N_c}{\pi} \tag{36}$$

which has the units of mass squared. In these dimensionless variables,

$$H\phi_n=\mu_n^2\phi_n, \quad n=0,1,2,\ldots. \tag{37}$$

The quark mass enters by the dimensionless parameter

$$\gamma=\frac{m_q^2}{e^2}. \tag{38}$$

The squared momentum P^2 is replaced by the dimensionless variable Q^2

$$Q^2=\frac{P^2}{e^2}. \tag{39}$$

The basic formulas for the meson propagators with massive quarks are

$$P_R(Q^2,\gamma)=\sum_{n\geqslant 0\ \text{even}}^{\infty}\left[\frac{r_n^2}{Q^2+\mu_n^2}-\frac{r_n^2}{\mu_n^2}\right]$$
$$S_R(Q^2,\gamma)=\sum_{n\geqslant 1\ \text{odd}}^{\infty}\left[\frac{r_n^2}{Q^2+\mu_n^2}-\frac{r_n^2}{\mu_n^2}\right]. \tag{40}$$

Asymptotically $\mu_n^2\sim\pi^2 n$, and the residues approach a finite limit, so the subtracted sums converge.

The residues r_n^2 are given in terms of the real, normalized wave functions $\phi_n(x)$:

$$r_n^2=\frac{1}{\pi}\gamma\left[\int_0^1 dx\,\frac{\phi_n(x)}{x}\right]^2. \tag{41}$$

For massless quarks, one needs to take the limit $\gamma\to 0$. The relevant combination is S_R+P_R, which is the regulated version of Eq. (27). For $m_q=0$, the lowest meson mass is zero, and there is an infrared divergence at $p=0$. This is handled by making the subtraction at nonzero Q^2. More information about H and the evaluation of Eq. (40) is collected in the Appendix.

C. Numerical results in the reduced model

We have focused on two cases. The first is $\gamma=1$ which, as explained in the Appendix, corresponds to an intermediate quark mass. The other case is massless quarks, where the chiral symmetry is spontaneously broken at weak g^2 coupling in the planar limit. Other values of γ are briefly discussed.

Numerical results are obtained by working in the "unitary gauge" and generating gauge fields T_1 that are related to Y by conjugation. Every conjugation belongs to an $SU(2)$ subgroup of $SU(N_c)$. A proposed conjugation is accepted or rejected by the Metropolis algorithm. The $SU(2)$ elements are picked so that the acceptance rate is close to 0.5. One iteration is defined as a sequence of attempted updates for an entire set of $N_c(N_c-1)/2$ $SU(2)$ subgroups of $SU(N_c)$. The subgroups in the set are defined by placing the $SU(2)$ matrix in the $(n,n),(n,m),(m,n),(m,m)$ entries of the $SU(N_c)$ T_1 matrix. The indices obey $1\leqslant n<m\leqslant N_c$. Fermionic measurements are made every 100 iterations, and 1000 iterations are used for thermalization.

Fermionic propagators are computed using Eq. (24). This is done by diagonalizing H_W exactly, constructing ϵ, and then performing an exact diagonalization of $\gamma_3\epsilon$. The propagator, $g(p_1,p_2)$, at any mass, is obtained from the spectral decomposition of $\gamma_3\epsilon$. This is done for all values of p_1 and p_2 and at a fixed value of T_1. The "bare" scalar and pseudoscalar propagators are

$$S_0(P)=\frac{1}{4N_c^2}\sum_{p_1,p_2}\mathrm{Tr}[g(p_1+P_1,p_2+P_2)g(p_1,p_2)$$
$$+g(p_1-P_1,p_2+P_2)g(p_1,p_2)$$
$$+g(p_1+P_2,p_2+P_1)g(p_1,p_2)$$
$$+g(p_1+P_2,p_2-P_1)g(p_1,p_2)] \quad (42)$$

$$P_0(P)=\frac{1}{4N_c^2}\sum_{p_1,p_2}\mathrm{Tr}[g(p_1+P_1,p_2+P_2)g^\dagger(p_1,p_2)$$
$$+g(p_1-P_1,p_2+P_2)g^\dagger(p_1,p_2)$$
$$+g(p_1+P_2,p_2+P_1)g^\dagger(p_1,p_2)$$
$$+g(p_1+P_2,p_2-P_1)g^\dagger(p_1,p_2)]. \quad (43)$$

There are different vectors $P=(P_1,P_2)$ which correspond to the same value of $P^2\equiv 4\Sigma_\mu \sin^2(P_\mu/2)$. By definition, the lattice meson propagators are a function of P^2 only. This function is obtained by averaging over all momenta with the same P^2. After a final average over several values of T_1, these propagators are the reduced model's approximation to Eq. (40).

We first compare numerical results to the continuum keeping $\gamma=1$ fixed. In order to study the approach to the continuum limit, we carried out simulations at five values of b^2: 1,2,3,4,5. At each value of b^2, we generated gauge field configurations at $N_c=31$, 37, and 41 to see how the limit $N_c=\infty$ is approached. The lattice momenta $\sqrt{P^2}$ range from 0 to $2\sqrt{2}$ while $\sqrt{Q^2}$, reaches a maximum of 7 at $b^2=1$ and a maximum of 16 at $b^2=5$. In this range of momenta, good estimates of $P_R(Q^2,1)$ and $S_R(Q^2,1)$ are obtained by including only the first 100 terms in the sum over states. Since we have included the first 2000 eigenvalues (see the Appendix), our ''theoretical'' data are very accurate.

Let $S_L(Q^2,1)$ and $P_L(Q^2,1)$ denote the regularized, reduced model scalar and pseudoscalar propagators. As in the continuum, we subtract the propagators at zero momentum. Data at $b^2=5$ are shown in Figs. 3 and 4. At lower values of b, the N_c dependence is even weaker. Even at $b^2=5$, we find that $N_c=41$ is large enough to provide accurate numbers for $N_c=\infty$.

We study the approach to the continuum limit in Figs. 5 and 6. Looking at different b^2 values, we see that the pseudoscalar propagator approaches its continuum limit more smoothly than the scalar propagator. For $\sqrt{Q^2}<4$, the numbers seem to have converged to their $b^2\to\infty$ limit, and there is reasonable agreement with the continuum result. On the other hand, the scalar propagator has not yet converged to its $b^2=\infty$ limit in any region of Q^2. It shows some overall agreement with continuum results, but it is less convincing than in the pseudoscalar case. In addition, the pseudoscalar propagator seems to approach its continuum limit monotonically, but the scalar propagator does not.

The main difference between the scalar and pseudoscalar propagators is that the lowest mass in the pseudoscalar channel is smaller than the lowest mass in the scalar channel. In the pseudoscalar propagator, we have agreement below

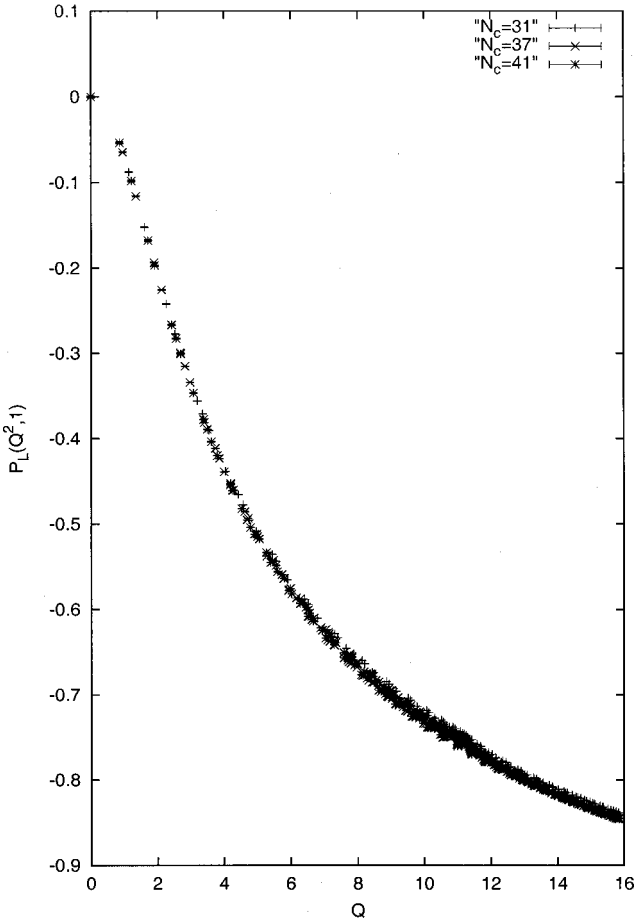

FIG. 3. Plot of $P_L(Q^2,1)$ at $b^2=5$ for $N_c=31,37,41$.

$\sqrt{Q^2}=4$, and the lowest pseudoscalar mass is $\mu_0=2.69713$, which is below $\sqrt{Q^2}=4$. However, the lowest scalar mass is $\mu_1=4.16036$, which is slightly above $\sqrt{Q^2}=4$. Hence, all the masses contributing to the scalar propagator are above the region of Q where the pseudoscalar propagator converged well to its continuum limit. Thus, the difference we found between the scalar and pseudoscalar propagators is likely to be a finite b^2 effect.

The difference between the two propagators can also be seen by extracting an effective mass. We set the momentum in one direction to zero and Fourier transform on the other component to produce a function of a conjugate, discrete ''spatial'' variable. Figure 7 is a semilogarithmic plot of the scalar and pseudoscalar propagators at sample parameter values $b^2=5$ and $N_c=41$. We see that the pseudoscalar propagator is a better fit to a straight line.

One can get an effective mass in either channel by forcing straight line fits. The resulting effective masses at $N_c=41$ are shown in Fig. 8 as a function of b^2. Although both masses appear to approach the correct continuum values, the finite b^2 effects on the scalar mass are much stronger.

We now turn our attention to the behavior of the pseudoscalar propagator as a function of m_q/e. We numerically computed this propagator as a function of $\sqrt{P^2}$ at several values of m_q/e for $b^2=5$ and $N_c=37$. An effective mass was extracted as before. This effective mass is plotted as a function of m_q/e in Fig. 9.

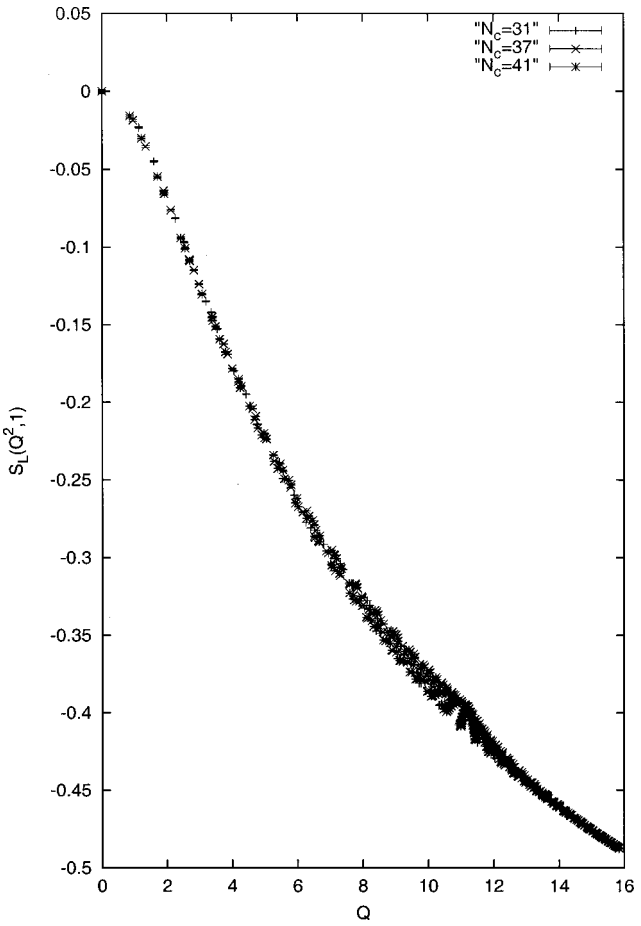

FIG. 4. Plot of $S_L(Q^2,1)$ at $b^2=5$ for $N_c=31,37,41$.

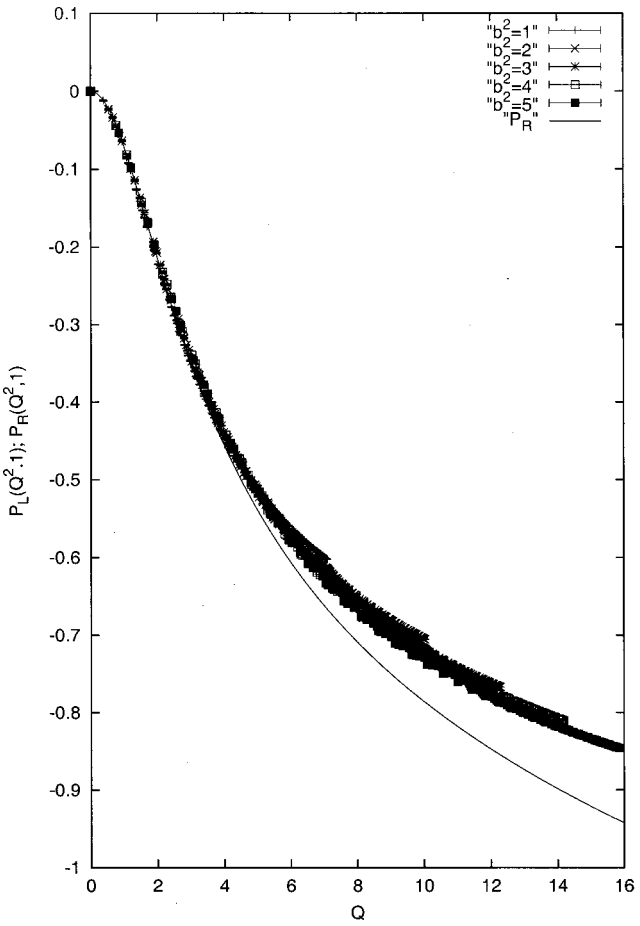

FIG. 5. Plot of $P_L(Q^2,1)$ at $N_c=41$ for $b^2=1,2,3,4,5$.

The empirical fit

$$\frac{m_\pi}{m_q}=2+0.51\left(\frac{m_q}{e}\right)^{-0.78} \tag{44}$$

shown in the plot works quite well.

With increasing m_q/e, the ratio m_π/m_q approaches 2, as expected. However, the subleading behavior does not match the expression derived in the Appendix which has -1.33 rather than -0.78 in the exponent. On the other hand, m_π/e is clearly not proportional to $\sqrt{m_q/e}$ as would be appropriate for light quarks. We get 0.78 instead of 0.5 in the exponent. The fit indicates that the masses we used are in an intermediate region.

Finally we look at massless quarks. To compare the lattice data to theory, we need to pick a subtraction point. We used $\sqrt{Q^2}=3$. For any finite N_c, the scalar and pseudoscalar propagators are identical for massless quarks. As explained earlier, the common value of these reduced model propagators ought to be compared with the continuum M_R defined by

$$M_R(Q^2)=\frac{1}{2\pi}\sum_{n\geqslant 0}^{\infty}\left[\frac{r_n^2}{Q^2+\mu_n^2}-\frac{r_n^2}{3^2+\mu_n^2}\right]. \tag{45}$$

The comparison for the subtracted meson propagator is shown in Fig. 10 and is quite good. The deviations that now appear at small Q can be mostly attributed to finite N_c effects which are sizable now because of the massless pseudoscalar mode.

IV. SUMMARY AND CONCLUSIONS

The main objective of this paper was to introduce a new program whose aim is the numerical solution of planar QCD. Our first test was an application to two-dimensional planar QCD. Much more can be done on this test case; our results are just the very first steps. We hope to carry out similar preparatory studies in four dimensions.

Our numerical experiment in two dimensions shows that reduction can reproduce some correct numbers, but that precise agreement would require a more substantial effort. It should be kept in mind that QCD_2 in the planar limit is quite challenging numerically. This model was chosen as our test case only because we have exact theoretical information about it. In four dimensions, the planar limit of QCD might be approached more rapidly.

Perhaps surprisingly, two dimensions might be even harder than four dimensions in the reduced model framework. If all minima of the pure gauge action are correctly sampled, $N_c\sim V^{1/d}$. Therefore, roughly, the number of inte-

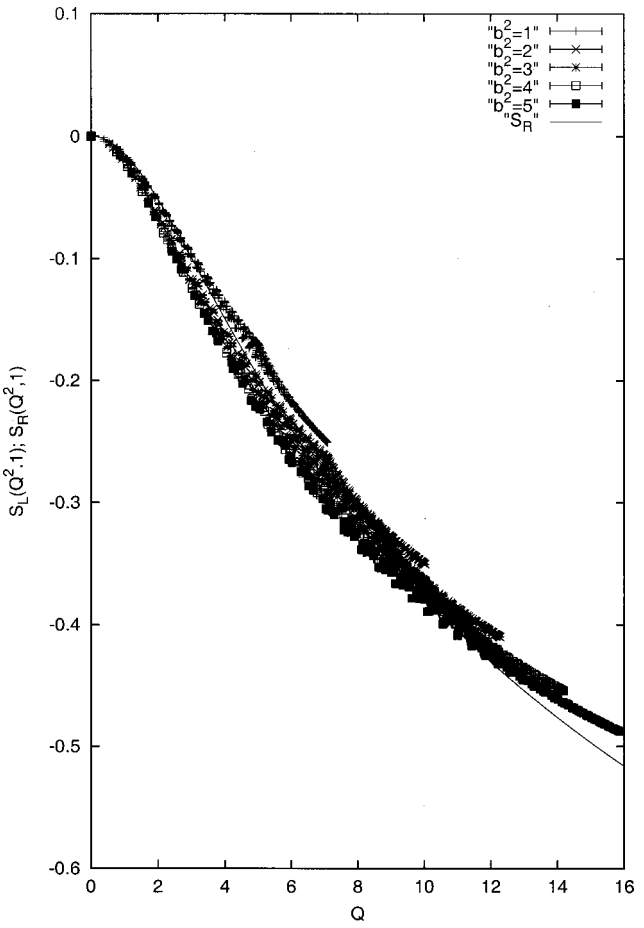

FIG. 6. Plot of $S_L(Q^2,1)$ at $N_c=41$ for $b^2=1,2,3,4,5$.

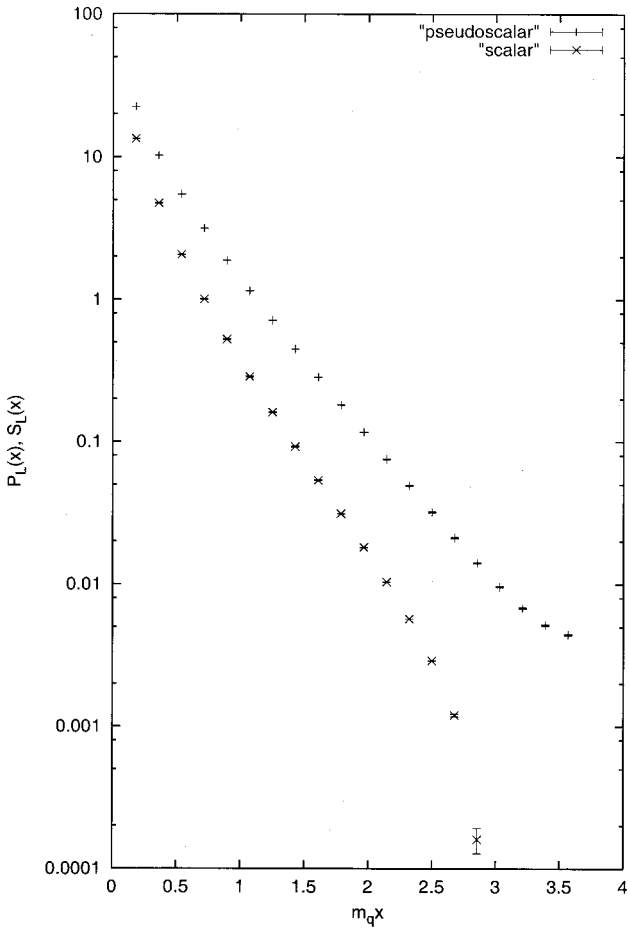

FIG. 7. Plot of the scalar and pseudoscalar propagators in real space at $b^2=5$ and $N_c=41$.

gration variables, N_c^2, decreases with the dimension at a fixed equivalent number of lattice sites. One might not need more lattice sites in four dimensions than in two because infrared effects are stronger in two dimensions.

The ultraviolet cutoff is increased by decreasing the 't Hooft scaled coupling e^2, which is the same as taking our b^2 parameter to infinity. Numerically we have learned that one needs larger N_c values to see convergence to the planar limit for larger values of b^2. The associated cost could be reduced by improving the lattice action and our fermionic operators. Already from [4], we learn that simple improvement methods have a beneficial effect. After reduction, the relative benefit from improvement might be less than in regular simulations. Of course, one needs to rethink what kind of algorithms are best suited for reduced models.

We have determined numerically that the eigenvalue distribution of the parallel transporters around plaquettes has support in only a small neighborhood of unity when we are at reasonably weak gauge coupling. As a result, the spectrum of the Wilson-Dirac operator develops a gap around zero. This in turn would speed up the numerical algorithms used to implement the lattice overlap propagators.

Reduction would also provide a means for evaluating $1/N_c$ corrections. Thus, one might not only get numbers in the planar limit but also an estimate for their accuracy in the context of real QCD. By going to the Veneziano limit instead of to the 't Hooft limit, we might get meson widths in addition to the meson masses. Recall that the momentum enters very differently here so that one might even contemplate a direct analytical continuation in momentum to physical values. The Veneziano limit, as a function of N_f/N_c, would provide quantitative assessments of the valence approximation—something of great value at this point in time.

Furthermore, the old problem of dealing with complex actions numerically might be more tractable in reduced models because the number of integration variables seems to be so much smaller. This would open new ways to look at θ dependence and at finite baryonic density. We conclude that pursuing our proposal further is a risk that is worth taking and look forward to further developments in this direction.

ACKNOWLEDGMENTS

The research of H.N. was supported in part by DOE grant DE-FG02-01ER41165. H.N. would like to thank the Guggenheim and Lady Davis Foundations for financial support. H.N. would like to thank V. Kazakov and the entire theory group at Ecole Normale, M. Moshe and the entire theory group at the Technion, and S. Nussinov and the entire theory group at Tel Aviv University for hospitality and sup-

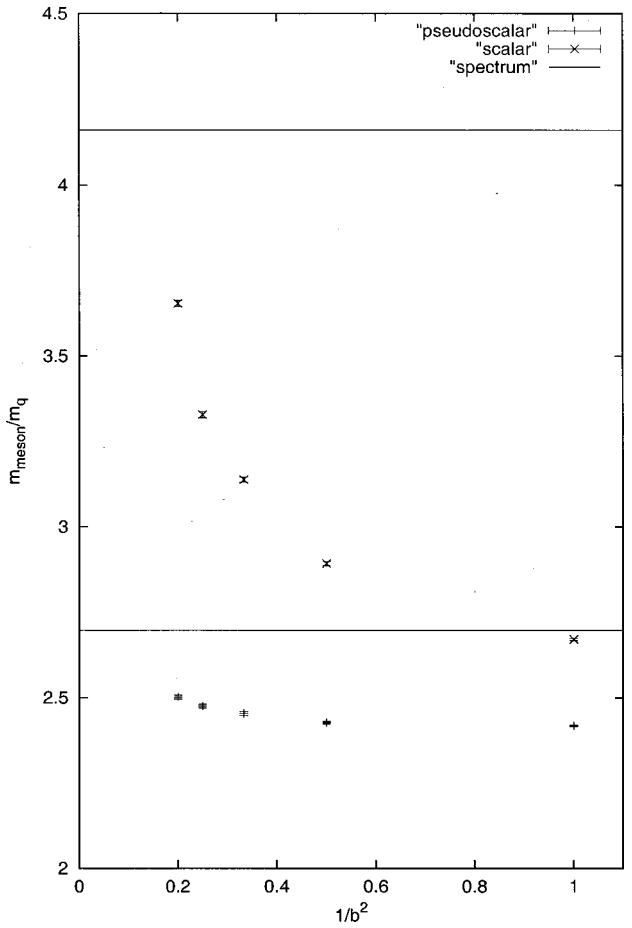

FIG. 8. Plot of the effective mass extracted from the scalar and pseudoscalar propagators as a function of b^2 at $N_c=41$.

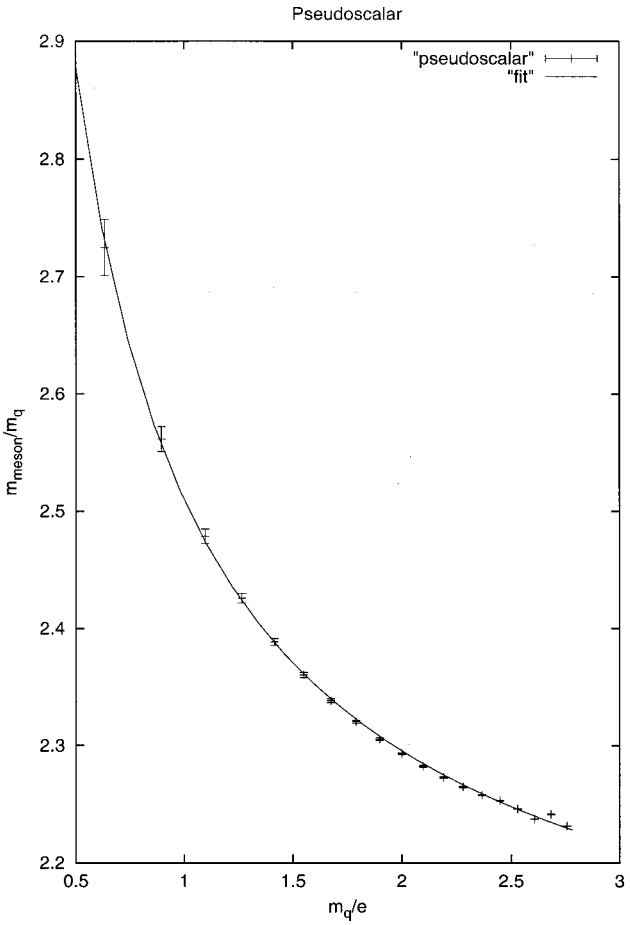

FIG. 9. Plot of the effective mass extracted from the pseudoscalar propagator as a function of m_q/e at $N_c=37$.

port. H.N. would also like to thank F. Berruto, L. Giusti, A. González-Arroyo, V. Kazakov, C. Rebbi, and M. Teper for discussions related to the topics of this paper. We also wish to acknowledge W. Krauth and M. Staudacher for help regarding numerical ways to obtain the 't Hooft exact solution. R.N. would like to acknowledge the DOE grant DE-FG02-01ER41165 for computational support. Part of the numerical work was done using the LINUX cluster located in the ITD of BNL. J.K. gratefully acknowledges access to the LINUX PC cluster of W. Pickett's condensed matter theory group at UC Davis where some of the calculations were done.

APPENDIX

In this appendix we describe the combination of numerical and analytical methods used to produce the theoretical predictions for the meson correlators. Without exception we are only dealing with the case of quarks of degenerate mass. Our presentation is fairly detailed.

The 't Hooft's Hamiltonian, H, is defined by

$$(H\phi)(x)=\gamma\left(\frac{1}{x}+\frac{1}{1-x}\right)\phi(x)-\int dy\,\frac{P}{(y-x)^2}\times[\phi(y)-\phi(x)]. \tag{A1}$$

1. Asymptotics of wave functions

There is an $x\to 1-x$ symmetry under which the eigenfunctions of H will be either even or odd. We wish to determine the correct boundary conditions on the wave functions and thus define the Hilbert space on which H acts. We shall focus on the $x=0$ end point. The above reflection about $x=\frac{1}{2}$ determines then the boundary conditions at the other end point.

We write $P/(y-x)^2=-(d/dy)[P/(y-x)]$ in Eq. (A1) and perform an integration by parts. Then, we add and subtract $\phi'(x)$ in the integral, ending up with

$$(H\phi)(x)=\gamma\left(\frac{1}{x}+\frac{1}{1-x}\right)\phi(x)+\frac{\phi(1)-\phi(x)}{1-x}-\frac{\phi(x)-\phi(0)}{x}-\frac{1}{2}\phi'(x)\log\left(\frac{1-x}{x}\right)^2-\int_0^1 dy\,\frac{\phi'(y)-\phi'(x)}{y-x}. \tag{A2}$$

We now assume asymptotics of the type

$$\phi(x)\sim x^\beta \quad \text{for } x\to 0. \tag{A3}$$

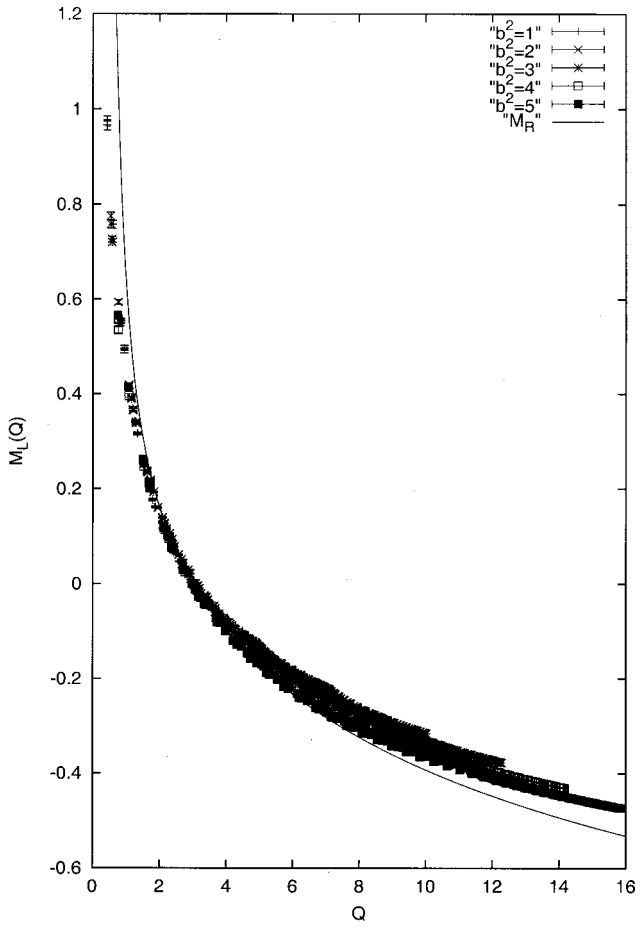

FIG. 10. Plot of the meson propagator for massless quarks as a function of b^2. The $b^2=1$ data are at $N_c=37$, the $b^2=2,4$ data are at $N_c=41$ and the $b^2=3,5$ data are at $N_c=47$.

We plug this in and evaluate for $x\sim 0$. We use the asymptotic form over the entire integration range inside the integral, but shall later make sure that only the region of y close to zero contributes to the final expression. Also assume that $0<\beta<1$. Then the two most singular terms at $x=0$ are contained in

$$(H\phi)(x)\sim(\gamma-1)x^{\beta-1}+\frac{\beta}{2}x^{\beta-1}\log x^2 - \beta x^{\beta-1}\int_0^{1/x} du\left[\frac{u^{\beta-1}-1}{u-1}+\frac{1}{u+1}\right] + \beta x^{\beta-1}\log\frac{1}{x}. \tag{A4}$$

Integration variables were changed in the integral: $y=ux$. The term $1/(u+1)$ was added and subtracted. The subtracted integral is trivial and gives the second term that contains a logarithm in Eq. (A4). The integral converges as the upper limit goes to infinity. Thus, even if we stop the integration at a large finite number A the answer would be some number which will depend on A only slightly. But, if A is finite, the range of y's is from zero to Ax, so it is all in the asymptotic regime. This is why we were justified in using the asymptotic expression for ϕ under the integral sign, for what seemed to be the entire range. The integral (for $x=0$) is done using the $\mu\to 1$ limit of

$$\int_0^\infty du\,\frac{u^{\beta-1}-u^{\mu-1}}{u-1}+\int_0^\infty du\,\frac{u^{\mu-1}}{u+1} = \pi(\cot\mu\pi-\cot\beta\pi)+\frac{\pi}{\sin(\mu\pi)} \tag{A5}$$

which is $-\pi\cot\pi\beta$.

The terms containing logarithms cancel and to cancel the subleading singularities (which are still too strong to be matched by a term linear in ϕ—which is what would be necessary for an eigenstate) we need

$$\gamma-1+\pi\beta\cot\pi\beta=0. \tag{A6}$$

This formula can be found in 't Hooft's original paper [3].

For light quarks, $\gamma\to 0$, and we get

$$\beta\sim\frac{1}{\pi}\sqrt{3\gamma}\quad\text{for}\quad\gamma\to 0. \tag{A7}$$

For massless quarks the asymptotic analysis needs to be redone. In this case the Hamiltonian has the constant function as the lowest eigenstate. Thus, the action of H on a function is determined by the derivative of the latter:

$$(H\phi)(x)=\frac{\phi(1)-\phi(x)}{1-x}-\frac{\phi(x)-\phi(0)}{x} -\frac{1}{2}\phi'(x)\log\left(\frac{1-x}{x}\right)^2-\int_0^1 dy\,\frac{\phi'(y)-\phi'(x)}{y-x}. \tag{A8}$$

We assume

$$\phi'(x)\sim x^\alpha\quad\text{for}\quad x\to 0 \tag{A9}$$

with $0<\alpha<1$ and check for consistency. This will give a condition on α, which will have a solution in the required interval. As before, we take the asymptotic form throughout the integration range, and leave it to the end to check that the contributions kept only came from the asymptotic regime. We find

$$(H\phi)(x)=-\frac{1}{1+\alpha}x^\alpha+x^\alpha\log x-x^\alpha\int_0^{1/x}du\,\frac{u^\alpha-1}{u-1}+\cdots. \tag{A10}$$

The u integral is rewritten by adding and subtracting terms chosen for their large u behavior, with the objective of isolating the contribution from the region near the end point $y=0$:

$$\int_0^{1/x} du\,\frac{u^\alpha-1}{u-1}=\int_0^{1/x} du\left[\frac{u^\alpha-1}{u-1}-u^{\alpha-1}+\frac{1}{u+1}\right]$$

$$+\frac{1}{\alpha x^\alpha}+\log\frac{x}{1+x}. \tag{A11}$$

Collecting terms in the integral and using

$$\int_0^\infty du u^{p-1}\frac{P}{1-u^q}=\frac{\pi}{q}\cot\frac{p\pi}{q}\quad\text{for}\quad p<q \tag{A12}$$

we get

$$\int_0^\infty \frac{u^\alpha+u^{\alpha-1}-2}{1-u^2}=\pi\cot(\pi\alpha). \tag{A13}$$

As a result, we get

$$(H\phi)(x)=-\frac{1}{\alpha}-\frac{x^\alpha}{\alpha+1}+\pi x^\alpha\cot\pi\alpha+\cdots. \tag{A14}$$

α is the unique solution between 0 and 1 of the equation:

$$\pi\cot\pi\alpha=\frac{1}{\alpha+1}. \tag{A15}$$

This equation is the same as Eq. (A6), extended to $1<\beta<2$, with $\beta=\alpha+1$ and with $\gamma=0$. Since the leading term is a constant, we see that the next period of the cotangent in Eq. (A6) provides the subleading behavior.

In summary we conjecture that the eigenfunctions for massive quarks have the following expansion near $x=0$:

$$\phi_n^\gamma(x)\sim(a_0^1x^{\beta_1}+a_1^1x^{\beta_1+1}+\cdots)+(a_0^2x^{\beta_2}+a_1^2x^{\beta_2+1}+\cdots)$$
$$+\cdots+(a_0^kx^{\beta_k}+a_1^kx^{\beta_k+1}+\cdots)+\cdots \tag{A16}$$

where β_k, $k=1,2,\ldots$ are, in increasing order, all the positive solutions of Eq. (A6). When the quark mass is taken to zero the entire series associated with the first root is replaced by a constant.

In the massless case we also can say that, for any excited eigenstate of H, $(H\phi_E)(x)=E\phi_E(x), E>0$ we have

$$\phi_E(x)=\mathcal{N}\left(1-\frac{\alpha E}{\alpha+1}x^{\alpha+1}\right)$$
$$+\text{terms that vanish faster as } x\to 0. \tag{A17}$$

The value of $0<\alpha<1$ can be easily calculated numerically. Note that the subleading correction at the end point holds in an ever decreasing range as the energy of the state, E, increases.

In conclusion, the Hilbert space appropriate to the Hamiltonian for the case of massless quarks consists of square integrable functions on the segment obeying von Neumann boundary conditions $\phi'(0)=\phi'(1)=0$. In the massive case, the boundary conditions were Dirichlet, $\phi(0)=\phi(1)=0$ instead. Note that the internal Hilbert spaces corresponding to massless and massive quarks are distinct, as one might have guessed would be appropriate for a manifestation of spontaneous symmetry breaking in the planar limit.

2. Massive quarks: $\gamma=1$

Equation (A6) simplifies when $\gamma=1$: its roots are $\beta_k=k-\frac{1}{2}$ with $k=1,2,\ldots$. The double series in Eq. (A16) collapses into a single series and $\phi_n^1(x)$ has the simple structure of $\sqrt{x}$ times a series in x for the $x\to 0$ asymptotic regime. For the eigenvectors, there is a $x\to 1-x$ symmetry, so the structure should be

$$\phi_n^1(x)=2\sqrt{x(1-x)}f_n(x) \tag{A18}$$

where f_n is either even or odd about the center of the segment (0,1). It is convenient to map this segment to $(-1,1)$.

For $\gamma=1$ the Hamiltonian is particularly simple:

$$(H\phi)(x)=-\int_0^1 dy\,\frac{P}{y-x}\phi'(y). \tag{A19}$$

Under the change of variables $x\to 2x-1$, and still using a prime to denote derivatives with respect to the new variable, we get

$$(H\phi)(x)=-2\int_{-1}^1 dy\,\frac{P}{y-x}\phi'(y). \tag{A20}$$

ϕ vanishes at the end points, so $\phi=$const is not an eigenstate. The eigenfunctions are defined over the segment $(-1,1)$ and have the structure (dropping the superscript denoting the value of γ)

$$\phi_n(y)=\sqrt{1-y^2}f_n(y). \tag{A21}$$

We shall use Chebyshev polynomials of the first (T) and second (U) kind to parametrize f_n [41]. Some of their properties are listed below:

$$U_n(\cos\theta)=\frac{\sin(n+1)\theta}{\sin\theta}$$

$$T_n(\cos\theta)=\cos n\theta$$

$$\int_{-1}^1 dy\,\frac{P}{y-x}\,\frac{T_n(y)}{\sqrt{1-y^2}}=\pi U_{n-1}(x)$$

$$\int_{-1}^1 dy\,\frac{P}{y-x}\sqrt{1-y^2}U_n(y)=-\pi T_{n+1}(x) \tag{A22}$$

$$\int_{-1}^1 dx\sqrt{1-x^2}U_n(x)U_m(x)=\frac{\pi}{2}\delta_{n,m}$$

$$2(x^2-1)U_{m-1}(x)U_{n-1}(x)=T_{n+m}(x)-T_{|n-m|}(x).$$

The indices n and m above are non-negative and vary in the ranges in which the equations make sense.

We represent a given function $\phi(y)$ as

$$\phi(y)=\sqrt{1-y^2}\sum_{n=0}^{\infty} a_n U_n(y). \tag{A23}$$

A short calculation then gives

$$\phi'(y)=-\frac{1}{\sqrt{1-y^2}}\sum_{n=0}^{\infty}(n+1)a_n T_{n+1}(y). \tag{A24}$$

Using the properties of the Chebyshev polynomials listed in Eq. (A22) we find

$$(H\phi)(x)=2\int_{-1}^{1}dy\,\frac{P}{y-x}\,\frac{1}{\sqrt{1-y^2}}\sum_{n=0}^{\infty}(n+1)a_n T_{n+1}(y)$$

$$=2\pi\sum_{n=0}^{\infty}(n+1)a_n U_n(x). \tag{A25}$$

Suppose $\phi(x)$ is an eigenstate of H with eigenvalue E, $(H\phi)(x)=E\phi(x)$. Then,

$$E\sqrt{1-y^2}\sum_{n=0}^{\infty}a_n U_n(y)=2\pi\sum_{n=0}^{\infty}(n+1)a_n U_n(y). \tag{A26}$$

One can proceed now by using orthogonality on one of the sides of the equation. We choose to multiply the equation by $\sqrt{1-y^2}U_m(y)$ and integrate over y:

$$E\sum_{n=0}^{\infty}a_n\int_{-1}^{1}dy(1-y^2)U_n(y)U_m(y)=\pi^2(m+1)a_m. \tag{A27}$$

We need to evaluate the integral on the left-hand side. Using an identity in Eq. (A22) we find

$$\int_{-1}^{1}(1-y^2)U_n(y)U_m(y)=\frac{1}{2}\int_{-1}^{1}[T_{|n-m|}(y)-T_{n+m+2}(y)]$$

$$\equiv\xi_{nm}=\xi_{mn}. \tag{A28}$$

By $y\to -y$ we see that $\xi_{nm}=0$ for $n-m$ odd. Also,

$$\sum_{n=0}^{\infty}\xi_{mn}a_n=\frac{\pi^2}{E}(m+1)a_m. \tag{A29}$$

We defined new coefficients

$$b_n=\sqrt{n+1}\;\;a_n. \tag{A30}$$

We also defined a new matrix X

$$X_{mn}=\frac{1}{\sqrt{m+1}}\xi_{mn}\frac{1}{\sqrt{n+1}}. \tag{A31}$$

We end up needing the eigenvalues of the symmetric matrix X:

$$\sum_{n=0}^{\infty}X_{mn}b_n=\frac{\pi^2}{E}b_m. \tag{A32}$$

To calculate the entries ξ_{mn} we go to angular variables, $y=\cos\theta$:

$$\xi_{mn}=\frac{1}{2}\int_0^{\pi}d\theta\sin\theta[\cos(n-m)\theta-\cos(n+m+2)\theta]. \tag{A33}$$

We need one elementary integral, for even integer k:

$$\int_0^{\pi}d\theta\sin\theta\cos k\theta=-\frac{2}{k^2-1}. \tag{A34}$$

For odd k the integral vanishes. This leads, for $n-m$ even, to

$$\xi_{mn}=\frac{1}{(n+m+2)^2-1}-\frac{1}{(n-m)^2-1}. \tag{A35}$$

In particular, on the diagonal we have

$$\xi_{nn}=1+\frac{1}{4(n+1)^2-1}. \tag{A36}$$

For $n-m$ odd the matrix element ξ_{mn} vanishes. The matrix X is given by

$$X_{mn}=\frac{1}{\sqrt{(m+1)(n+1)}}\times\left[\frac{1}{(n+m+2)^2-1}-\frac{1}{(n-m)^2-1}\right] \tag{A37}$$

for $n-m$ even and $X_{mn}=0$ for $n-m$ odd. If λ is an eigenvalue of X, $E=\pi^2/\lambda$ is an eigenvalue of the 't Hooft Hamiltonian.

For high states one can use the diagonal terms as an approximation. One gets the asymptotic estimate

$$E_n\sim\pi^2(n+1) \tag{A38}$$

with the state label n starting at $n=0$.

We need to determine the normalization convention on the infinite vectors $(b_0,b_1,\ldots)$ that would make the eigenstates $\phi_E(x)$ $(H\phi_E=E\phi_E)$ normalized to unity by $\int_0^1\phi_E^2(x)=1$. $\phi_E(x)$ is parametrized by

$$\phi_E(x)=2\sqrt{x(1-x)}\sum_{n=0}^{\infty}\frac{b_n^E}{\sqrt{n+1}}U_n(2x-1) \tag{A39}$$

where x is in the original range $(0,1)$. Introducing the expansion we find

$$1=\frac{\pi^2}{2E}\sum_{n=0}^{\infty}(b_n^E)^2 \tag{A40}$$

where

$$\sum_{n=0}^{\infty} X_{mn} b_n = \frac{\pi^2}{E} b_m . \tag{A41}$$

We are now ready to compute the residues for $\gamma = 1$. We need to calculate

$$\rho_n^1 = \int_0^1 \frac{dx}{x} \phi_n(x). \tag{A42}$$

Here, γ was set to unity and the eigenfunction is assumed correctly normalized. Changing variables, we arrive at

$$\rho_n^1 = \sum_{k=0}^{\infty} a_k^{(n)} I_k \tag{A43}$$

with

$$I_k = \int_0^{\pi} d\theta \frac{\sin\frac{\theta}{2}}{\cos\frac{\theta}{2}} \sin(k+1)\theta. \tag{A44}$$

We change the integration variable θ to $\pi - \theta$ and average the expressions. Then, for k even we have to calculate

$$I_k = \int_0^{\pi} d\theta \frac{\sin(k+1)\theta}{\sin\theta}. \tag{A45}$$

Use

$$\frac{\sin(k+1)\theta}{\sin\theta} = \sum_{j=0}^{k} e^{\imath(k-2j)\theta} \tag{A46}$$

to conclude that for even k only the $j = k/2$ term in the sum makes a contribution, giving

$$I_k = \pi. \tag{A47}$$

For k odd

$$I_k = -\int_0^{\pi} d\theta \frac{\sin(k+1)\theta}{\sin\theta} \cos\theta. \tag{A48}$$

By the same technique as above we get non-zero contributions only from $j = (k \pm 1)/2$ (for odd k, $k \geqslant 1$). Hence, for k odd:

$$I_k = -\pi. \tag{A49}$$

Only the absolute value of ρ_n^1 is determined, since the sign of the wave function is not fixed by normalization. The final answer is

$$|\rho_n^1| = \pi \left| \sum_{k \geqslant 0,\ k-n=\text{even}} \frac{b_k^{(n)}}{\sqrt{k+1}} \right|. \tag{A50}$$

Here, the normalization condition is

$$\sum_{k \geqslant 0,\ k-n=\text{even}} (b_k^{(n)})^2 = \frac{2E^{(n)}}{\pi^2}. \tag{A51}$$

In each sector the eigenvalues were obtained numerically by diagonalizing a truncation of the infinite matrix X of Eq. (A31). The residues were obtained using Eq. (A50) with the eigenfunctions of the truncated matrix X normalized according to Eq. (A51). In each sector a matrix of size 2000×2000 was diagonalized and this produced accurate estimates of the lowest 1000 eigenvalues in that sector. The lowest pole contributing to the pseudoscalar is at $\mu_0 = 2.69713$ and the lowest pole contributing to the scalar is at $\mu_1 = 4.16036$. Asymptotically, the eigenvalues are given by $\mu_n^2 = \pi^2 n + \frac{3}{4}\pi^2 + \mathcal{O}1/n$. The residues, r_n^2, reach an asymptotic value of π^2. The even residues approach this number monotonically from above ($r_0^2 = 11.7596864$) and the odd residues approach this number monotonically from below ($r_1^2 = 9.03541704$).

3. Massless quarks

We now turn to the evaluation of eigenvalues and residues in the case of massless quarks. The correct boundary conditions for the massless case are von Neumann so we choose to diagonalize the Hamiltonian in the basis of cosine functions:

$$\langle x|n\rangle = \sqrt{2}\cos\pi n x, \quad n \geqslant 1; \quad \langle x|0\rangle = 1. \tag{A52}$$

The states are numbered, starting with 0. The ground state is known exactly and by keeping $n \geqslant 1$ we are in a space orthogonal to it. Just as before, even and odd n states do not mix, so we can diagonalize the Hamiltonian in each of these subspaces separately,

$$\begin{aligned}\langle n|H|m\rangle = &\int_0^1 dx \int_0^1 dy \int_0^{\infty} t dt e^{-t|x-y|} \\ &\times [\cos(\pi n x) - \cos(\pi n y)] \\ &\times [\cos(\pi m x) - \cos(\pi m y)].\end{aligned} \tag{A53}$$

To do the integrals we introduce, with no restriction on the integers n, m, the integral

$$\begin{aligned}I_{n,m} = &\frac{1}{2}\int_0^1 dx \int_0^1 dy \int_0^{\infty} t dt e^{-t|x-y|} [e^{\imath\pi n x} - e^{\imath\pi n y}] \\ &\times [e^{\imath\pi m x} - e^{\imath\pi m y}].\end{aligned} \tag{A54}$$

By changing variables $x \to 1-x$ and $y \to 1-y$ we see that

$$I_{n,m} = (-1)^{n+m} I_{n,m}^* . \tag{A55}$$

We now restrict ourselves to even $n+m$. This is enough to get all nonzero matrix elements $\langle n|H|m\rangle$. In this case we learn that $I_{n,m}$ is real,

$$I_{n,m}+I_{n,-m}=\int_0^1\int_0^1\int_0^\infty tdte^{-t|x-y|}[e^{\imath\pi nx}-e^{\imath\pi ny}]\times[\cos(\pi mx)-\cos(\pi my)]. \tag{A56}$$

But, since $I_{n,m}$ is real we can take the real part to prove

$$\langle n|H|m\rangle=I_{n,m}+I_{n,-m}. \tag{A57}$$

We need only $I_{n,m}$ for $n+m$ even. Using the symmetry under exchange of x and y we get

$$I_{n,m}=\int_0^1 dx\int_0^x dy\int_0^\infty tdte^{-t(x-y)}[e^{\imath\pi nx}-e^{\imath\pi ny}]\times[e^{\imath\pi mx}-e^{\imath\pi my}]. \tag{A58}$$

Using the above, and restricting in the end to $n,m\geqslant 1$ and even $n+m$ we get

$$\langle n|H|m\rangle=\pi^2 n\,\delta_{n,m}+2\int_0^\infty tdt\Bigg\{[1+(-1)^{n-1}e^{-t}]\times\Bigg[\frac{1}{t^2+\pi^2n^2}+\frac{1}{t^2+\pi^2m^2}-\frac{\pi^2(n^2+m^2)}{(t^2+\pi^2n^2)(t^2+\pi^2m^2)}\Bigg]-(1-e^{-t})\Bigg[\frac{1}{t^2+\pi^2(n+m)^2}+\frac{1}{t^2+\pi^2(n-m)^2}\Bigg]\Bigg\}. \tag{A59}$$

The matrix elements of H can be expressed in terms of sine-integral and cosine-integral functions. For $n\neq m$, with $n+m$ even:

$$\langle n|H|m\rangle=\log\left(\frac{n^2-m^2}{nm}\right)^2+\frac{n^2+m^2}{n^2-m^2}\log\left(\frac{m}{n}\right)^2+\frac{4}{n^2-m^2}[n^2\mathrm{ci}(\pi n)-m^2\mathrm{ci}(\pi m)]-2\{\mathrm{ci}[\pi(n+m)]+\mathrm{ci}[\pi(n-m)]\}. \tag{A60}$$

For $n=m$:

$$\langle n|H|n\rangle=\pi^2 n-2\log n+\log\frac{4}{\pi^2}-2(1+\gamma)+2[\pi n\,\mathrm{si}(\pi n)+(-1)^n]+4\,\mathrm{ci}(\pi n)-2\,\mathrm{ci}(2\pi n). \tag{A61}$$

One needs to distinguish between Si, Ci and si, ci. Here are the definitions for the functions used in Eqs. (A60) and (A61):

$$\mathrm{si}(x)=-\int_x^\infty dt\frac{\sin t}{t}=-\frac{\pi}{2}+\int_0^x dt\frac{\sin t}{t}=-\frac{\pi}{2}+\mathrm{Si}(x) \tag{A62}$$

$$\mathrm{ci}(x)=-\int_x^\infty dt\frac{\cos t}{t}=\mathrm{Ci}(x). \tag{A63}$$

The asymptotics go as follows: For integer and large positive k

$$\mathrm{ci}(\pi k)=\frac{(-1)^{k-1}}{(\pi k)^2}+\mathcal{O}\left(\frac{1}{(\pi k)^4}\right)$$

$$\mathrm{si}(\pi k)=\frac{(-1)^{k-1}}{\pi k}+\mathcal{O}\left(\frac{1}{(\pi k)^3}\right). \tag{A64}$$

To find the residues in the case of massless quarks one needs to take the $\gamma\to 0$ limit on the massive formula:

$$\rho_n^\gamma=\sqrt{\gamma}\int_0^1 dx\frac{\phi_n^\gamma(x)}{x}. \tag{A65}$$

$\phi_n^\gamma(x)$ is the nth (ordered by eigenvalue and starting from $n=0$) normalized eigenstate of the Hamiltonian with mass parameter γ.

The entire contribution comes from the lower end of the integral, because only from there does one get a singularity in γ that can compensate the vanishing prefactor. Thus, only the asymptotic behavior of the wave function is needed. It is given by

$$\phi_n^\gamma(x)=A_n^\gamma x^{\beta(\gamma)}+\text{ terms that vanish faster as } x\to 0. \tag{A66}$$

Hence,

$$\rho_n^0=\frac{\pi}{\sqrt{3}}A_n^0. \tag{A67}$$

In general, A_n^0 is difficult to obtain, as it is fixed by the normalization of the wave function and depends on its values throughout the interval. But, for $n=0$ we know that, at small γ, $\phi_0(x)$ tends to 1. Hence, $A_0^0=1$ and we get

$$\rho_0^0=\frac{\pi}{\sqrt{3}}. \tag{A68}$$

For arbitrary n we need to compute numerically the nth wave function for the massless case, normalize it, and get A_n^0 from its values at the end point,

$$A_n^0=\phi_n^0(0). \tag{A69}$$

A sign ambiguity remains, as the sign of the wave function remains undetermined by the normalization condition. But, only $(\rho_n^0)^2$ enters in the amplitude so everything is well determined.

The eigenvalues were obtained from a truncation of H in Eq. (A53) to size 1000×1000 in each sector. The residues are obtained from the end point of the normalized eigenvector as given by Eq. (A67). The lowest non-zero eigenvalue is a scalar meson (having an antisymmetric wave function) at $\mu_1=2.4233$ and its residue is $r_1^2=7.58941916$. Asymptotically, the eigenvalues are described by $\mu_n^2=\pi^2 n-2\log(n)+O(1)$. The constant term is close to $\frac{1}{2}\pi^2$ but due to the $\log(n)$ term it is hard to determine it accurately. The residues are relatively difficult to estimate due to slow convergence. They asymptote to $r_n^2=\pi^2$ and are monotonic in n.

4. Light versus heavy quarks

We wish to determine whether $\gamma=1$ should be viewed as a light quark mass or as a heavy quark mass. To do this we first find the leading behavior of the pion mass for very small quark masses. This behavior has the typical structure induced by spontaneous chiral symmetry breaking. We then compare the leading chiral approximation to the pion mass with the exact value. If the quarks are light the approximation should work well numerically. If the quarks are heavy the approximation should be off. We also compute the pion mass for very heavy quarks. Again we compare the approximate expression to the exact value.

To compute the pion mass ($n=0$ state) to leading order in the assumed small quark mass we start from

$$\begin{aligned}(\mu_0^\gamma)^2&=\int_0^1 dx\,\phi_0^\gamma(x)(H\phi_0^\gamma)(x)\\&=\gamma\int_0^1[\phi_0^\gamma(x)]^2\left(\frac{1}{x}+\frac{1}{1-x}\right)\\&\quad-\int_0^1 dx\int_0^1 dy\frac{P}{(y-x)^2}\phi_0^\gamma(x)[\phi_0^\gamma(y)-\phi_0^\gamma(x)].\end{aligned}\tag{A70}$$

We symmetrize both terms, the first under parity $x\to1-x$, the second under interchange of x with y, to get

$$(\mu_o^\gamma)^2=2\gamma\int_0^1\frac{[\phi_0^\gamma(x)]^2}{x}+\frac{1}{2}\int_0^1 dx\int_0^1 dy\left[\frac{\phi_0^\gamma(y)-\phi_0^\gamma(x)}{y-x}\right]^2.\tag{A71}$$

As $\gamma\to0$ the first term is dominated by the end point contribution. Actually, also the second term is dominated by the end point contribution. As before, we use the asymptotic behavior throughout the integration range, but ascertain at the end that we were dominated by the end points. From the first term we get a contribution:

$$\frac{\pi}{\sqrt{3}}\sqrt{\gamma}+\mathcal{O}(\gamma).\tag{A72}$$

The second term requires more work:

$$\frac{1}{2}\int_0^1 dx\int_0^1 dy\left[\frac{y^\beta-x^\beta}{y-x}\right]^2=\frac{1}{2}\int_0^1 dx\,x^{\beta-1}\int_0^{1/x}du\left[\frac{u^\beta-1}{u-1}\right]^2.\tag{A73}$$

The u integral is done extending the upper limit to infinity. The correction needed to account for this approximation will be of higher order in β. The u integral is done as follows: Write $[1/(u-1)]^2=-(d/du)[1/(u-1)]$ and do the integral by parts to obtain

$$\begin{aligned}\int_0^\infty du\left[\frac{u^\beta-1}{u-1}\right]^2&=-1-2\beta\int_0^\infty du\,\frac{u^{2\beta-1}-u^{\beta-1}}{1-u}\\&=-1-2\beta\pi[\cot(2\beta\pi)-\cot(\beta\pi)]\\&=\frac{2}{3}(\beta\pi)^2+\mathcal{O}(\beta^4).\end{aligned}\tag{A74}$$

Doing the remaining x integral we learn that the double integral gives a contribution equal to that of the first term.

In summary we get, converting to physical units:

$$m_\pi^2=2m_q|g|\sqrt{\frac{\pi N}{3}}+\mathcal{O}(m_q^2).\tag{A75}$$

This is the result found by 't Hooft [42]. Equation (A75) can be rewritten in variables rendered unitless by using g^2N/π as a mass-square scale as

$$\begin{aligned}\mu_\pi^2&=\sqrt{\gamma}\frac{2\pi}{\sqrt{3}}\\\frac{m_\pi}{m_q}&=\frac{\mu_\pi}{\sqrt{\gamma}}=\sqrt{\frac{2\pi}{\sqrt{3}}}\gamma^{-1/4}\approx\frac{1.90}{\gamma^{1/4}}.\end{aligned}\tag{A76}$$

For $\gamma=1$ we found numerically that $m_\pi/m_q=2.7$ establishing that $\gamma=1$ corresponds to quite light quarks, but still the $\mathcal{O}(m_q^2)$ corrections to Eq. (A75) make a substantial contribution.

The pion is, by definition, the lowest energy eigenstate of the 't Hooft Hamiltonian in the sector of functions symmetric under $x\to1-x$.

For γ large the first term in the 't Hooft Hamiltonian dominates, so the pion wave function will try to minimize its contribution by being concentrated around the point $x=\frac{1}{2}$. Making the wave function too narrow incurs a price from the second term. This suggests a variational estimate for the leading and subleading order in $1/\gamma$. The trial wave function is

$$\phi(x)=\left(\frac{\lambda}{\pi}\right)^{1/4}[e^{-(\lambda/2)[x-(1/2)]^2}-e^{-\lambda/8}].\tag{A77}$$

$\phi(x)$ is normalized to unity up to corrections that are exponentially small in λ.

The expectation value of the 't Hooft Hamiltonian in the state ϕ is

$$\langle\phi|H|\phi\rangle=\gamma\int_0^1\left(\frac{1}{x}+\frac{1}{1-x}\right)\phi^2(x)+\frac{1}{2}\int_0^1 dx\int_0^1 dy\left[\frac{\phi(y)-\phi(x)}{y-x}\right]^2. \quad \text{(A78)}$$

Contributions from the end points of the integral in the first term are exponentially small in λ and will be neglected, under the assumption (to be later justified) that λ diverges as $\gamma\to\infty$. Thus we can calculate the contribution of the first term by infinite range Gaussian integration, obtaining

$$4\gamma+\frac{8\gamma}{\lambda}+\mathcal{O}(\lambda^{-2}). \quad \text{(A79)}$$

The second term is

$$\frac{1}{2}\sqrt{\frac{\lambda}{\pi}}\int_0^1 dx\int_0^1 dy\left[\frac{e^{-(\lambda/2)[x-(1/2)]^2}-e^{-(\lambda/2)[y-(1/2)]^2}}{x-y}\right]^2. \quad \text{(A80)}$$

The integral (excluding the prefactor) has a finite $\lambda\to\infty$ limit:

$$\int_{-\infty}^{\infty}du\int_{-\infty}^{\infty}dv\left(\frac{e^{-u^2/2}-e^{-v^2/2}}{u-v}\right)^2. \quad \text{(A81)}$$

The expression $(u-v)^2$ in the denominator is represented by an integral over t of $e^{-t(u-v)^2}$ from zero to infinity. The u,v integrals of each one of the terms can be done by Gaussian integration, and calculating the appropriate 2×2 determinants one finds that the above integral is given by

$$2\pi\int_0^{\infty}\left[\frac{1}{\sqrt{t}}-\frac{1}{\sqrt{t+\frac{1}{4}}}\right]=2\pi. \quad \text{(A82)}$$

Hence

$$\langle H\rangle\sim4\gamma+\frac{8\gamma}{\lambda}+\sqrt{\pi\lambda}. \quad \text{(A83)}$$

Extremizing on λ gives

$$\lambda=\left(\frac{16}{\sqrt{\pi}}\right)^{2/3}\gamma^{2/3}. \quad \text{(A84)}$$

Thus, indeed λ is large for γ large and the wave function is close to a delta function around $x=\frac{1}{2}$. For the unitless pion mass square we find

$$\mu_\pi^2\sim4\gamma+(16\pi)^{1/3}\frac{3}{2}\gamma^{1/3}. \quad \text{(A85)}$$

For large γ we expect, therefore,

$$\frac{m_\pi}{m_q}\sim2(1+0.69\gamma^{-2/3}). \quad \text{(A86)}$$

Using this formula blindly for $\gamma=1$ gives $m_\pi/m_q\sim3.4$ instead of the true value of 2.7. We see that the true value is midway between the leading answer corresponding to light pions (1.9) and the leading plus subleading expression valid for heavy quarks. Thus, $\gamma=1$ corresponds to intermediate gauge coupling (in units of quark mass).

[1] G. 't Hooft, Nucl. Phys. **B72**, 461 (1974); E. Witten, *ibid.* **B160**, 57 (1979); S. Coleman, lectures at the 1979 International School of Subnuclear Physics, Erice, Italy, 1979.
[2] G. 't Hooft, Commun. Math. Phys. **81**, 267 (1981).
[3] G. 't Hooft, Nucl. Phys. **B75**, 461 (1974).
[4] M. Teper, Nucl. Phys. B (Proc. suppl.) **109**, 134 (2002), and references therein; an earlier indication for fast approach to $N_c=\infty$ is by S.A. Chin and M. Karliner, Phys. Rev. Lett. **58**, 1803 (1987).
[5] F. Berruto, L. Giusti, C. Hoelbling, and C. Rebbi, Phys. Rev. D **65**, 094516 (2002).
[6] T. Eguchi and H. Kawai, Phys. Rev. Lett. **48**, 1063 (1982).
[7] D. Kessler and H. Neuberger, Phys. Lett. **157B**, 416 (1985); H. Neuberger, Nucl. Phys. **B340**, 703 (1990).
[8] G. Eyal, M. Moshe, and J. Zinn-Justin, Nucl. Phys. **B470**, 369 (1996).
[9] G. 't Hooft, Commun. Math. Phys. **88**, 1 (1983).
[10] G. Bhanot, U.M. Heller, and H. Neuberger, Phys. Lett. **112B**, 47 (1982).
[11] D. Gross and Y. Kitazawa, Nucl. Phys. **B206**, 440 (1982).
[12] A.A. Migdal, Phys. Lett. **116B**, 425 (1982).
[13] G. Parisi, Phys. Lett. **112B**, 463 (1982).
[14] A. González-Arroyo and M. Okawa, Phys. Lett. **120B**, 174 (1983); Phys. Rev. D **27**, 2397 (1983); T. Eguchi and R. Nakayama, Phys. Lett. **122B**, 59 (1983).
[15] A. González-Arroyo and C.P. Korthals Altes, Phys. Lett. **131B**, 396 (1983).
[16] H. Levine and H. Neuberger, Phys. Lett. **119B**, 183 (1982).
[17] V. Kazakov and A.A. Migdal, Phys. Lett. **119B**, 435 (1982).
[18] G. Veneziano, Nucl. Phys. **B117**, 519 (1976).
[19] S.R. Das, Phys. Lett. **132B**, 155 (1983).
[20] H. Levine and H. Neuberger, Phys. Rev. Lett. **49**, 1603 (1982).
[21] H. Neuberger, Phys. Lett. **119B**, 179 (1982); H. Neuberger, Nucl. Phys. **B220**, 237 (1983).
[22] W. Bardeen, A. Buras, and J.-M. Gérard, Nucl. Phys. **B293**, 787 (1987).
[23] D.B. Kaplan, Phys. Lett. B **288**, 342 (1992); R. Narayanan and H. Neuberger, *ibid.* **302**, 62 (1993); Phys. Rev. Lett. **71**, 3251 (1993); Nucl. Phys. **B443**, 305 (1995); H. Neuberger, Phys. Rev. D **57**, 5417 (1998); Annu. Rev. Nucl. Part. Sci. **51**, 23 (2001).
[24] E. Witten, Phys. Rev. Lett. **81**, 2862 (1998) and references therein.
[25] R.G. Edwards, U.M. Heller, and R. Narayanan, Nucl. Phys. **B535**, 403 (1998).
[26] H. Neuberger, Phys. Rev. D **61**, 085015 (2000).

[27] H. Neuberger, Phys. Lett. B **417**, 141 (1998); **427**, 353 (1998).
[28] D.H. Adams, J. Math. Phys. **42**, 5522 (2001).
[29] H. Neuberger, in *Lattice Fermions and the Structure of the Vacuum*, edited by V. Mitrjushkin and G. Schierholz (Kluwer Academic, Dordrecht, 2000), pp.113–124.
[30] D. Gross and E. Witten, Phys. Rev. D **21**, 446 (1980).
[31] A.A. Migdal, M.I. Polikarpov, A.I. Veselov, and V.P. Yurov, Phys. Lett. **135B**, 145 (1984).
[32] L. Giusti, A. González-Arroyo, C. Hoelbling, H. Neuberger, and C. Rebbi, Phys. Rev. D **65**, 074506 (2002).
[33] A. González-Arroyo, *Gauge Fields on the Four-dimensional Torus*, Proceedings of the Peñiscola 1997 Advanced School on Non-Perturbative Quantum Field Physics (World Scientific, Singapore, 1998).
[34] H. Neuberger, Phys. Lett. **94B**, 199 (1980).
[35] H. Neuberger, Phys. Rev. D **59**, 085006 (1999).
[36] H. Neuberger, Nucl. Phys. B (Proc. Suppl.) **73**, 697 (1999).
[37] R.G. Edwards, U.M. Heller, and R. Narayanan, Phys. Rev. D **59**, 094510 (1999).
[38] A.R. Zhitnitsky, Phys. Rev. D **53**, 5821 (1996) and references therein; I. Affleck, Nucl. Phys. **B265[FS15]**, 448 (1986); C.J. Hammer, *ibid.* **B195**, 503 (1982).
[39] Y.Y. Goldschmidt, Phys. Lett. **119B**, 174 (1982).
[40] C.G. Callan, N. Coote, and D.J. Gross, Phys. Rev. D **6**, 1649 (1976).
[41] A. Hanson, R. Peccei, and M. Prasad, Nucl. Phys. **B121**, 477 (1977); R.C. Brower, W.L. Spence, and J.H. Weis, Phys. Rev. D **19**, 3024 (1979).
[42] G. 't Hooft, in *New Phenomena in Subnuclear Physics, Part A*, Proceedings of the International School of Subnuclear Physics, Erice, 1975 edited by A. Zichichi (Plenum, New York, 1977), Vol. 1.